JOURNAL OF GEOPHYSICAL RESEARCH, VOL. 105, NO. B5, PAGES 11,153–11,169, MAY 10, 2000

Shallow mantle temperatures under Europe from *P* and *S* wave tomography

S. Goes[1] and R. Govers

Vening Meinesz Research School of Geodynamics, Utrecht University, Utrecht, Netherlands

P. Vacher

Laboratoire Geophysique et Planétologie, Université de Nantes, Nantes, France

Abstract. Temperature is one of the key parameters controlling lithospheric and mantle dynamics and rheology. Using recent experimental data on elastic parameters and anelasticity, we obtain models of temperature at 50 to 200 km depth beneath Europe from the global *P* wave velocity model of *Bijwaard et al.* [1998] and the regional *S* wave velocity model of *Marquering and Snieder* [1996]. Forward modeling of seismic velocity allows us to assess the sensitivity of velocity to various parameters. In the depth range of interest, variations in temperature (when below the solidus) yield the largest effects. For a 100°C increase in temperature, a decrease of 0.5-2% in V_P and 0.7-4.5% in V_S is predicted, where the strongest decrease is due to the large effect of anelasticity at high temperature. The effect of composition is expected to give velocity anomalies <1% for the shallow mantle and would therefore be difficult to resolve. At depths >80 km the relative amplitudes of the European V_P and V_S anomalies are consistent with a thermal origin. At shallower depths, variations in crustal thickness and possibly the presence of partial melt appear to have an additional effect, mainly on *S* wave velocity. In regions where both *P* and *S* anomalies are well-resolved, V_P- and V_S-derived thermal models agree well with each other and with temperatures determined from surface heat flow observations. Furthermore, the thermal models are consistent with known tectonics. The inferred temperatures vary significantly, from around 400°C below an average mantle adiabat at 100 km depth under the Russian Platform and a 300°C increase from east to west across the Tornquist-Teisseyre zone to temperatures around the mantle adiabat in the depth range 50-200 km under areas with present surface volcanism. In spite of the uncertainties in the calculation of temperatures due to uncertainties in the experimental elastic parameters and anelasticity and uncertainties associated with tomographic imaging, we find that the tomographic models of the shallow mantle under Europe can yield useful estimates of the thermal structure.

1. Introduction

Temperature is one of the key parameters controlling lithospheric and mantle dynamics and rheology. Except in some boreholes, no direct measurements of temperature at depth are available. There are, however, several indirect ways of obtaining information on temperature inside the Earth.

In the lithosphere where heat transport is conductive, temperature at depth can be estimated through the extrapolation of surface heat flow observations [e.g., *Cermák and Bodri*, 1995; *Pollack and Chapman*, 1977]. This requires assumptions on the distribution of crustal heat production and the variation of thermal conductivity with depth [e.g., *Chapman*, 1986]. One problem is that surface heat flow data may be dominated by the effect of very shallow and local sources, for example, circulation of hydrothermal fluids, thus hampering the estimate of temperatures in the deeper lithosphere.

Where xenoliths of the right composition are available, geothermobarometry can be used to construct a geotherm for the lithosphere and sometimes shallow mantle [e.g., *O'Reilly et al.*, 1990; *Sobolev et al.*, 1997]. Geothermobarometry works in areas where there are sufficient samples to allow for well-constrained estimates of pressure and temperature, with a large enough spread in depth [*O'Reilly et al.*, 1990]. The xenoliths reflect the effects of the geotherm at the time when volcanism brought them up to the surface and are not necessarily representative of the present-day thermal state of the lithosphere. When the samples can also be dated, geothermobarometry may yield additional information on the evolution of the geotherm through time [*O'Reilly and Griffin*, 1996].

Seismic waves allow for three-dimensional imaging of seismic velocity in the Earth's interior. In addition to the major discontinuities which represent compositional changes (phase and/or chemical transitions), much of the three-dimensional mantle velocity structure in the upper mantle can probably be attributed to variations in temperature [*Forte et al.*, 1994; *Ranalli*, 1996]. Quantifying the thermal structure responsible for the observed velocity anomalies would therefore give a much more complete picture of temperature in the Earth than other data can. Furthermore, time lag uncertainties which are intrinsic to heat flow and

[1]Now at Institut für Geophysik, Eidgenössische Technische Hochschule, Zurich, Switzerland.

Copyright 2000 by the American Geophysical Union.

Paper number 1999JB900300.
0148-0227/00/1999JB900300$09.00

geothermobarometry do not affect seismic velocities which represent present-day structure. Uncertainties related to tomographic imaging, especially in the recovery of the amplitude of seismic anomalies, can hamper the estimate of the responsible variations in temperature. Spatial resolution and smearing of anomalies which are strongly dependent on the distribution of stations and sources are an additional problem. With the continuously improving quality of data and tomographic methods and availability of P and S velocity models for the same regions, estimates of thermal structure are becoming feasible in more areas. It is the purpose of this paper to explore the conversion from seismic velocity to temperature for the shallow mantle under Europe.

Several factors other than temperature can influence seismic velocity, for example, composition, presence of partial melt or water, and anisotropy. Forward modeling of seismic velocity for a given thermal and compositional structure can be done using the large amount of experimental data on elastic moduli and density for all important mantle and many crustal minerals (see compilations by *Bass* [1995], *Duffy and Anderson* [1989], *Sumino and Anderson* [1984], *Vacher et al.* [1998]). Such modeling has shown that the effect on seismic velocity of compositional variations in the uppermost mantle (inferred from the more abundant types of xenoliths) is probably (much) smaller than the effect of thermal variations [*Jackson and Rigden*, 1998; *Jordan*, 1979]. *Griffin et al.* [1998], however, claim that compositional variations in continental lithospheric mantle may account for a significant part of the observed seismic velocity anomalies. The effect of anelasticity, often not included, strongly amplifies the sensitivity of seismic velocity to temperature [*Karato*, 1993]. If P and S waves have a different sensivity to temperature and, for example composition, combining information from both wave types may allow us to distinguish between the effects of different parameters.

Previous efforts to infer temperature and/or composition from seismic velocities have used both forward modeling and inverse approaches. Using experimentally derived parameters for the main mantle minerals and their high pressure phases, velocity jumps in transition zone have been modeled [*Duffy and Anderson*, 1989; *Duffy et al.*, 1995; *Jackson and Rigden*, 1998; *Vacher et al.*, 1996, 1998]). In this way, one-dimensional velocity profiles can be fit, although these models have not been able to conclusively resolve the average composition of the upper mantle. Synthetic velocity models calculated from independently derived three-dimensional (predominantly thermal) mantle structure compare quite well with those obtained with tomography [*de Jonge et al.*, 1994; *Nataf and Ricard*, 1996], especially when the imaging procedures applied to the data are also applied to the synthetic models [*de Jonge et al.*, 1994; *Ricard et al.*, 1996]. The global synthetic mantle velocity model of *Nataf and Ricard* [1996] includes anelasticity and gives a good fit of several types of body and surface wave data [*Ricard et al.*, 1996]. *de Jonge et al.* [1994] use only anharmonic velocity derivatives to convert thermal anomalies into velocity anomalies. They do obtain a good agreement with tomography because their study focused on subducting slabs where the anelastic contribution is relatively small.

Reasonable results of forward modeling studies have motivated attempts to solve the inverse problem. *Yan et al.* [1989] set up an inversion of velocity variations for thermal structure and iron content. Since they used only shear wave velocities, the inversion could not solve for both parameters but only for the end-members of purely thermal or purely compositional variations. The global upper mantle thermal structure found was grossly consistent with observed heat flow. *Forte et al.* [1995, 1994] combined seismic and geoid (gravity) data to image both shear wave velocity and density variations in the mantle. Although their approach did not involve an inversion for temperature, they found that both the S wave and geodynamic data were consistent with the $\partial \ln \rho / \partial \ln V_S$ derived by *Karato* [1993] on the assumption of thermal variations only. In a more detailed study on continental roots, *Forte et al.* [1995] conclude that density at depths $\leq$250 km, as constrained by shear velocity, geoid, and dynamic topography, is predominantly the result of thermal effects. In the upper mantle below this depth a difference in chemistry between subcontinental and suboceanic mantle may also play a (stabilizing) role [*Forte et al.*, 1995]. *Furlong et al.* [1995] set up a combined inversion of P and S wave velocities to solve for temperature and variations in iron content. Unreasonably large variations in iron content were obtained in an application to Europe, possibly due to the different imaging techniques and resolution of the P and S models used. Another attempt at combining P and S velocity models by *Tralli and Ita* [1995], who computed tectonically regionalized variations in bulk velocity in the upper mantle, was probably also hampered by inconsistencies between the P and S models. All the inversion approaches above (except the work of *Forte et al.* [1995, 1994]) neglected the effect of anelasticity. In a more local study, *Sobolev et al.* [1996, 1997] try to account for all known effects on seismic velocity in the shallow mantle, except seismic anisotropy, in an inversion of a P velocity model under the Massif Central for thermal structure. Composition was based on data from xenoliths. Laboratory-derived anharmonic effects, anelastic effects, and effects of partial melting on temperature derivatives were included. Additional constraints from heat flow or heat flow and thermobarometry of xenoliths were used to constrain an average reference geotherm for their inversion. No information from shear waves was used by *Sobolev et al.* [1996, 1997].

In the present study we summarize the sensitivity of both compressional and shear wave velocities to the various parameters, temperature, composition, anelasticity, and partial melt by forward modeling of velocity and velocity derivatives using parameters from laboratory experiments. On the basis of the results of the forward calculations, tomographic models of both P and S wave velocity in the European lithosphere and shallow mantle are independently inverted for thermal structure. Our inversion approach is similar to the one taken by *Sobolev et al.* [1996, 1997] but includes both P and S waves and is applied on a regional scale. Europe is chosen because high-quality tomographic models are available both for P and S waves (e.g., the most recent P and S velocity models by *Bijwaard et al.* [1998] and *Marquering and Snieder* [1996]). Our focus is on the shallow mantle where the temperatures have a very direct effect on the dynamics of the lithosphere and surface observables (e.g., surface heat flow). For the deeper mantle the effect of phase transitions would need to be included [e.g., *Vacher et al.*, 1998] and the uncertainties increase due to the extrapolation of laboratory data. Comparison of the thermal models derived

independently from P and S velocities allows for validation of the procedure and the assumption that velocities are mainly affected by thermal variations. Where differences between the thermal models can not be attributed to imaging effects, the presence of melt or variations in composition may be responsible.

2. Forward Modeling of Seismic Velocities

Over the years, many laboratory measurements of density ρ and elastic parameters (compressibility K and rigidity or shear modulus μ) of the main rock-forming minerals at various pressures and temperatures have been made, allowing for the calculation of anharmonic seismic velocities for various compositions with reasonable confidence (see, for example, compilations by *Bass* [1995], *Duffy and Anderson* [1989], and *Sumino and Anderson* [1984]). In some cases, seismic velocities of bulk rock samples are measured directly [*Jackson et al.*, 1990; *O'Reilly et al.*, 1990; *Sato et al.*, 1989]. These velocities, measured at ultrasonic frequencies, agree well with the anharmonic velocities calculated using experimental parameters for individual minerals [*Jackson et al.*, 1990].

Anharmonic velocities neglect the effect of internal friction (or attenuation) and are thereby independent of frequency. Although the Earth behaves almost elastic at seismic frequencies, the occurrence of velocity dispersion and attenuation of seismic waves shows that anelastic effects, which cause a frequency dependence, are not negligible. Theoretical calculations [*Karato*, 1993] and experimental work (e.g., review by *Karato and Spetzler* [1990, and references therein] have shown that anelasticity can significantly affect (the temperature dependence of) velocities at seismic frequencies. Although the experimental data set on anelasticity is not as good as the data on elastic parameters and density (due to the experimental difficulty of anelasticity measurements), an estimate of the effect of anelasticity as a function of temperature, pressure, and frequency can be made based on these data.

The effect of the presence of melt on seismic velocity is probably large [*Sato et al.*, 1989; *Schmeling*, 1985] but not well constrained by either experimental or theoretical results. The main uncertainty is due to the strong dependence on melt geometry. Experiments on the distribution of basaltic melts [*Faul et al.*, 1994] show most melt to be present in low aspect ratio inclusions, which would imply a relatively strong effect on seismic velocity. A further complication is that the presence of water strongly affects the melting temperature. The difference between the water-saturated and dry mantle solidi increases from ~300°C at 50 km depth to ~700°C at 200 km depth [e.g., *Thompson*, 1992].

Water may be present in the uppermost mantle in hydrated minerals or possibly as free water [e.g., *Kawamoto and Holloway*, 1997]. Hydration of a rock can significantly alter seismic velocities. For example, the hydrous mineral phlogopite, which has been found in amounts as high as 10% in mantle xenoliths [*Waters and Erlank*, 1988], has a velocity about 30% lower than any of the main minerals which make up a peridotite [*Roosendaal*, 1998]. Formation of even small amounts of free water through the dehydration of hydrous minerals is known to significantly lower seismic velocities in crustal rocks [*Popp and Kern*, 1993]. Other work [*Karato and Jung*, 1998] suggests that water reduces mantle seismic velocities through enhanced anelasticity. The effect of water, direct or indirect, may thus be large, but the results available at present do not allow us to quantify the effect on seismic velocity.

Olivine is a strongly anisotropic mineral, and preferential alignment of the minerals (for example, due to flow) may cause anisotropic seismic velocities. Models of anisotropic P and/or S velocity have been made for parts of Europe [e.g., *Babuska et al.*, 1993; *Bormann et al.*, 1996], but not with the same spatial resolution and covering the same area as the isotropic velocity models used in this study. Because of the many uncertainties still associated with anisotropic seismic velocity models and because forward modeling of anisotropic seismic velocity (including temperature and pressure effects) still needs further experimental and theoretical developments, the effect of anisotropy will be neglected in this study. In section 2.1 our forward modeling procedure is explained, and using simple one-dimensional models, the sensitivity of seismic velocities to variations in temperature, composition, and partial melt is estimated in section 2.2.

2.1. Method

2.1.1. Anharmonicity. To calculate the anharmonic part of the velocities, we use the infinitesimal strain approximation, which is a reasonable approximation for depths to ~200 km [*Leven et al.*, 1981]. The effect on the velocities of using more correct finite strain theory is ~0.5%, which is small compared to the uncertainty of both the tomographic velocity models and the experimental parameters used for the forward modeling of velocities (see section 4.1). To estimate seismic velocities for rocks of a given mineralogical composition, Voigt-Reuss-Hill averaging of the parameters for the individual minerals is used. (This gives the same average values as the more accurate Hashin-Shtrikman averaging but is less laborious to calculate [*Vacher et al.*, 1996].) Most density and elastic parameters and their derivatives are available from experimental data (many of them already compiled [*Bass*, 1995; *Duffy and Anderson*, 1989; *Vacher et al.*, 1998]). Some of the temperature derivatives of the elastic moduli are not directly constrained by laboratory measurements but instead are based on structural and chemical trends [*Duffy and Anderson*, 1989] and are thus more uncertain. The equations used are summarized in the appendix, and Table A1 lists the parameters values used and estimates of their uncertainties.

2.1.2. Anelasticity. Seismological observations [e.g., *Anderson and Given*, 1982; *Anderson and Hart*, 1978] indicate that in the Earth, attenuation for shear deformation (Q_μ) is much stronger than for dilatational deformation (Q_K). To evaluate the effect of Q_μ, we use two models (see the appendix for the equations used). Q_1 is a Q model derived by *Sobolev et al.* [1996] (their model 2 with frequency exponent a = 0.15), where values averaged for the range of experimental results were used for the frequency exponent a and activation energy H^* and activation volume V^* and the pre-exponential constant A was set to match seismological attenuation observations. Q_2 is a completely experimental Q model for synthetic forsterite [*Berckhemer et al.*, 1982]. Table A2 lists the parameters used for the two Q models. Since no anelasticity data for different minerals are available, we cannot properly account for composition or assess how important the

effect of composition on attenuation parameters is. However, the available experimental data are obtained for various samples of synthetic forsterite, dunite, lherzolite, and peridotite [*Karato and Spetzler*, 1990], and the range given by the two Q models thus also includes a possible effect of composition.

Figure 1 shows Q obtained with the two models for a relatively warm geotherm (an average mantle adiabat with potential temperature 1280°C [*McKenzie and Bickle*, 1988]) and for a relatively cold geotherm which is representative of stable shield areas [*Chapman*, 1986] (continental geotherm for a surface heat flow of 40 mW/m^2). The larger activation energy and larger frequency exponent of model Q_2 [*Berckhemer et al.*, 1982] predicts Q effects that are relatively strong compared to those from other experiments (see *Karato and Spetzler* [1990] for a review). The model by *Sobolev et al.* [1996] can be considered a more average Q model. Anharmonic velocities represent a minimum effect of Q (equivalent to taking $Q \rightarrow \infty$).

Both experimental Q models give average values in the range of those observed seismically (Figure 1). For example, for Rayleigh waves at depths between 100 and 200 km, Q values of 40 to 70 are found in active areas, and $Q \approx$ 125-150 under shields [*Mitchell*, 1995] with no strong frequency dependence. Similar shield Q values were found under the Eurasian shield for 0.02 to 1 Hz body waves [*Der et al.*, 1986]. The one-dimensional global model ABM [*Anderson and Given*, 1982] lists Q_S (1 s) = 200, Q_S (100 s) = 100 for the depth range 50-200 km. The range in Q predicted by the experimental models is large; however, it is not inconsistent with seismic models that resolve regional variations in Q. Under Africa, *Xie and Mitchell* [1990] find variations in Q_{Lg} between ~350 and almost 1000, while a Q_S model for the Japanese slab and overlying wedge [*Sato*, 1992; *Umino and Hasegawa*, 1984] gives Q varying from 50 to >2000. To calculate Q_P, we take a constant Q_K = 1000 from the radial attenuation model by *Durek and Ekström* [1996] but assume $Q_P = Q_\mu = Q_S$, where Q_μ becomes larger than 1000 to ensure large Q values in the cold lithosphere.

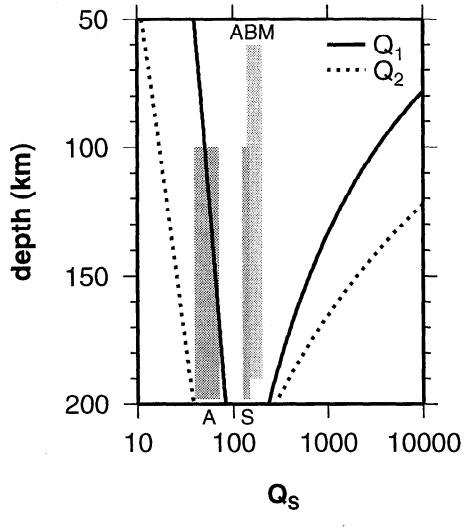

Figure 1. Comparison of the two Q models based on experimental parameters (Table A2) with estimates of Q from seismic waves (dark shading, for active (A) and shield (S) regions [*Mitchell*, 1995]; light shading, global model ABM [*Anderson and Given*, 1982]). For each model, S wave anelasticity is shown along a mantle adiabat with potential temperature of 1280°C (lines with the lowest Q), and a 40 mW/m^2 continental geotherm (high Q lines). A frequency of 0.05 Hz was used. Model Q_2 predicts stronger effects than Q_1. Both models give a relatively large range of Q values as a function of temperature.

2.2. Sensitivity

Table 1 summarizes the sensitivity of P and S wave velocity to temperature, composition and partial melt. Values of partial derivatives along an average mantle adiabat (potential temperature 1280°C) are given at depths of 50 and 200 km. The ratio $\partial \ln V_S / \partial \ln V_P$ provides an estimate of the relative sensitivity of V_P and V_S to the various parameters.

2.2.1. Temperature. The temperature sensitivity of anharmonic velocities does not vary significantly within the depth range considered here, but anelastic effects make $\partial \ln V / \partial T$ strongly dependent on temperature and pressure (Table 1). The equations used for calculating partial derivatives are given in the appendix. The effect of temperature is stronger for S than for P waves; the total $\partial \ln V_P / \partial T$ is ≈1-2% per 100°C, while the total $\partial \ln V_S / \partial T$ is estimated to be between 1% and >4% per 100°C (Table 1). The anharmonic derivatives provide an estimate of $\partial \ln V_{P,S} / \partial T$ under low-temperature conditions, and the total derivatives for a mantle adiabat provide a high-temperature estimate. Considering only anharmonic effects, we find $r = \partial \ln V_S / \partial \ln V_P$ = 1.3-1.4, adding anelasticity results in r = 1.7 for Q_1 [*Sobolev et al.*, 1996] and r = 1.8-2.0 using the Q_2 model [*Berckhemer et al.*, 1982] (Table 1). These numbers are close to those found from seismological velocity models. For the upper part of the mantle *Robertson and Woodhouse* [1997] find $r \approx$ 1.6 from P and S station corrections; in the upper 200 km of the mantle *Kennett et al.* [1998] find an average r of 2.2 to ~1.9. The agreement with our calculated r indicates that velocity anomalies in the uppermost mantle can largely be explained by variations in temperature alone. The additional effect of melt and variations in iron content can further increase r.

2.2.2. Composition. Previous workers have already shown that for reasonable variations in uppermost mantle composition (as constrained by compositions of xenoliths) the variations in velocity are relatively small [*Jackson and Rigden*, 1998; *Jordan*, 1979; *Sobolev et al.*, 1996] and often below the level that can be resolved with seismic tomography. For example, as peridotites melt, both garnet (the fastest mineral) and clinopyroxene (the slowest of the four major minerals) concentrate in the melt [e.g., *Niu* 1997], resulting in only minor changes in velocity (*Jordan* [1979], *Roosendaal* [1998], and Table 1, difference between primitive peridotite and depleted continental lherzolite).

Griffin et al. [1999, 1998] have documented a variation in composition of subcontinental lithosphere with thermotectonic age from xenoliths, garnet concentrates, and peridotite massifs and calculate that the seismic velocities for the different compositions do vary significantly. However, in addition to a compositional effect, the velocity difference between Archean and tectonic regions of *Griffin et al.* [1999] includes a temperature difference of 400 to 500°C. The earlier velocity estimates of *Griffin et al.* [1998] were only for room pressure and more recently *Griffin et al.* [1999] improved their

Table 1. Sensitivity of V_P, V_S to Temperature, Composition, and Melt

		$\partial \ln V_P/\partial Y$		$\partial \ln V_S/\partial Y$			$\partial \ln V_S/\partial \ln V_P$	
∂Y	Note	50 km	200 km	50 km	200 km	Unit	50 km	200 km
∂T_{anharm} [a]		-0.59	-0.48	-0.78	-0.69	%/100 K	1.32	1.43
$\partial T_{anh+anel}$ [a]	Q_1 [b]	-1.15	-0.75	-2.07	-1.34	%/100 K	1.80	1.79
	Q_2 [b]	-2.24	-0.96	-4.58	-1.84		2.04	1.92
∂X [c]	acsl [d]	-0.68		-0.77		%		
	pgp [d]	0.52	0.42	0.02	0.06			
	arch [d]	0.63	0.49	0.70	0.61			
	prot [d]	0.18	-0.05	-0.34	-0.46			
	tect [d]	0.05	-0.02	-0.58	-0.61			
∂X_{Fe} [e]	acgl [d]	-2.58	-2.38	-3.73	-3.47	%/0.1	1.44	1.45
	pgp [d]	-2.22	-2.07	-3.22	-3.01		1.45	1.45
∂X_{ol} [f]	acgl [d]	-0.04	0.22	0.32	0.46	%/0.1	-8.41	2.12
	pgp [d]	0.08	0.27	0.24	0.35		3.26	1.30
∂C_m [g]	$\partial \mu$ = -1	-0.53	-0.43	-0.76	-0.64	%/%	1.43	1.49
	$\partial \mu$ = -10	-3.70	-3.07	-8.50	-7.12		2.30	2.32

All partial derivatives are calculated for a mantle adiabat with a potential temperature of 1280 °C.

[a] For acgl.

[b] Q_1 [*Sobolev et al.*, 1996], Q_2 [*Berckhemer et al.*, 1982]. See text for further explanation of the two Q models. A frequency of 1 Hz is used.

[c] This compositional derivative ∂X is calculated as $(V_{comp}-V_{acgl})/V_{acgl}$, where comp stands for an alternative composition, e.g., acsl or pgp.

[d] Here acgl is average continental garnet lherzolite [*Jordan*, 1979], olivine/orthopyroxene/clinopyroxine/garnet (ol/opx/cpx/gt) = 67/23/4.5/5.5%, Mg/(Mg+Fe) = 90; acsl, average continental spinel lherzolite [*McDonough*, 1990], ol/opx/cpx/sp = 62/24/12/2%, Mg/(Mg+Fe) = 90; pgp, primitive garnet peridotite [*McDonough*, 1990], ol/opx/cpx/gt = 58/18/10/14%, Mg/(Mg+Fe) = 89; arch, Archaen subcontinental lithosphere [*Griffin et al.*, 1999], ol/opx/cpx/gt = 69/25/2/4%, Mg/(Mg+Fe) = 93; prot, Proterozoic subcontinental lithosphere [*Griffin et al.*, 1999], ol/opx/cpx/gt = 70/17/6/7%, Mg/(Mg+Fe) = 91; tect, subcontinental lithosphere below tectonic regions [*Griffin et al.*, 1999], ol/opx/cpx/gt = 60/17/11/12%, Mg/(Mg+Fe) = 90.

[e] X_{Fe} = 0.0 is equivalent to Mg/(Mg+Fe) = 100, X_{Fe} = 0.1 to Mg/(Mg+Fe) = 10. When $\partial \ln V/\partial X_{Fe} < 0$ velocity decreases with increasing Fe content.

[f] X_{ol} = 1.0 means 100% olivine, X_{ol} =0.6 means 60% olivine and 40% (opx+cpx+gt). When $\partial \ln V/\partial X_{ol}$ >0, velocity increases with increasing olivine content.

[g] C_m is amount of melt in %. $\partial K/\partial C_m$ = 1 GPa/% melt; $\partial \mu = \partial \mu/\partial C_m$ in GPa/% melt.

method for calculating seismic velocities. None of the velocity estimates include the effect of anelasticity. We used their compositions [*Griffin et al.*, 1999] to calculate the effect of composition alone, at 50 and 100 km depth (Table 1). The differences between the velocity for our reference composition for continental lithosphere [*Jordan*, 1979] and the velocities for the different tectonic regions are <1%. Using both the geotherms and compositions of *Griffin et al.* [1999], composition contributes up to 25% of the difference in V_P and up to 35% of the difference in V_S between tectonic and Archean regions. These are, however, maximum effects. The part attributable to composition is only up to 10% of the difference in velocity between Proterozoic and tectonic regions. Given the resolution of current tomographic models, only the extreme difference in composition between tectonic and Archean regions may have a resolvable effect. Only a small part of the region considered in our subsequent study is of Archean age.

In an attempt to parametrize composition, we calculated two different compositional derivatives: one with respect to the amount of olivine, which is expected to increase with the amount of depletion of a mantle rock, and one with respect to the amount of iron, which will also increase as melt is extracted from a peridotite. We estimate that an increase in olivine content of 10% of the total volume results in a decrease of seismic velocity of the order of one tenth to at most a few tenths of a percent (Table 1). Varying the amount of olivine can result in very different effects on P and S wave velocities (Table 1). This is partially due to nonlinear behavior associated with our choice of the parameter X_{ol} where all other minerals were lumped together in an $X_{rest} = 1\text{-}X_{ol}$. The large variation in v is partially the result of dividing by a small $\partial \ln V_P/\partial X_{ol}$. The small variations in V_P and V_S predicted by changes in X_{ol} cannot be resolved in current tomographic models.

A decrease in iron content has a larger effect [*Jordan*, 1979]. Increasing the magnesium number, Mg/(Mg+Fe), by 10 is estimated to give a velocity increase of 2 to 3%. *Jordan* [1979] estimates that the extraction of 20% melt from a pyrolite results in a change in magnesium number of only 2.4, from 88.8 to 91.2. The effect of Fe is larger on S waves than on P waves with $v_{Fe} \approx$ 1.4-1.5 (Table 1).

Clearly, composition has a complex effect on seismic velocity which is not easily parametrized. In general, these calculations show that the effect of composition on seismic velocity is expected to be relatively small compared to the effect of temperature.

2.2.3. Partial melt. While the change in composition of peridotite as melt is extracted does not appear to significantly affect seismic velocities, the presence of melt is expected to have a large effect, owing to a strong decrease especially in the shear modulus. Although not much melt is expected to be present in the mantle, up to a few percent melt may accumulate before separation of melt occurs [*McKenzie*

and Bickle, 1988]. The effect of partial melt on seismic velocities depends strongly on geometry of the melt and whether or not melt pockets are interconnected [*Mavko*, 1980]. Experimental work [*Sato et al.*, 1989] at ultrasonic frequencies indicates a small amount of melt (>2%) needs to be present before an effect on the seismic velocities is found. For slightly larger amounts of melt, *Sato et al.* [1989] find a drop in V_P of ~1% per percent melt. Modeling by *Schmeling* [1985] predicts a decrease in bulk modulus of the order of 1 GPa per percent melt and a 1-10 GPa decrease in shear modulus per percent melt, where the different values are for various shapes of the melt inclusions, with aspect ratios between 1 and 0.01, respectively. Aspect ratios between 1 and 0.01 predict a 0.5-3.5% decrease of V_P per percent melt, and 0.7-8.5% decrease of V_S per percent melt (Table 1). Again, shear wave velocity is more sensitive than compressional wave velocity. The ν estimates range from 1.4 to 2.4. Experimental results [*Faul et al.*, 1994] on the melt distribution of ultramafic partial melts show that most melt resides in inclusions with aspect ratios <0.1. This result was found to be independent of the amount of melt present at least for the experiments with up to 3.2% melt performed by *Faul et al.* [1994] and predicts a relatively strong effect of the presence of partial melt.

Experiments [*Sato et al.*, 1989; *Berckhemer et al.*, 1982] indicate that Q does not significantly change upon crossing of the solidus [*Karato and Spetzler*, 1990]. Thus anelastic effects besides those due to the high temperatures necessary for melting are probably not important (at least for a few percent of melt).

2.2.4. Bulk/shear velocity anomalies. Another variable used to measure the different responses of P and S velocity separates the effect of bulk and shear modulus by using $\zeta = \ln\phi/\ln V_S$, where ϕ is bulk velocity. Although this separation of bulk and shear modulus information is desirable, the calculation of this parameter requires compatible P and S velocity models in order to avoid mapping different imaging artifacts into ζ. *Kennett et al.* [1998] calculated ζ from their combined global P and S wave inversion and found a large variation in ζ ranging from values smaller than -1 to larger than +1 in the uppermost mantle. The synthetic calculations done here predict ζ to be in the range +0.1 to +0.6 under shallow mantle conditions. For a ν between 1 and 2.3, which encompasses most of the effects investigated here (Table 1), ζ would be between 0 (for $\nu \approx 2.3$) and +1 (for $\nu = 1$). Opposite effects on bulk and shear velocity were only found as a result of some variations in composition (Table 1). However, the variations in velocity leading to very large or negative ζ were always small and would be difficult to resolve reliably by seismic tomography. Other effects (water?) not investigated here or different imaging effects for P and S waves could be responsible for the very large or negative values of ζ that *Kennett et al.* [1998] found for some regions in the shallow mantle. The anticorrelated bulk and shear wave anomalies might, for example, be the result of mapping an intrinsically anisotropic region into an isotropic tomographic model.

3. Temperatures Under Europe

After reviewing and quantifying the effect of different parameters on seismic velocities we concentrate on thermal effects. Seismic velocities are strongly dependent on variations in temperature (Table 1), and significant temperature variations are expected in the depth range of interest. While the effects of partial melt are expected to be very strong, they cannot be quantified with much confidence, since the derivatives of seismic velocity with respect to both the amount of melt and the amount of water (which controls the position of the solidus) are not well known. The effects of composition are expected to be much smaller (section 2.2.2., Table 1) than those of either temperature or melt in the depth range considered here. Given the uncertainties in the forward calculation of velocities due to uncertainties in the experimental parameters and uncertainties in the amplitudes of imaged velocity anomalies, an inversion for any other parameter than temperature is not warranted at present. We set up a procedure to invert P or S wave velocity images for temperature. P and S velocity models are inverted separately, and comparison of the results on scale lengths resolved by both models allows us to evaluate how good the assumption of mapping all variation in seismic velocities into thermal structure is. Where temperatures reach the solidus, the possibility of partial melt has to be considered.

In the tomographic models it has been assumed that velocity structure is isotropic. Anisotropic seismic velocities have been mapped under Europe [e.g., *Babuska and Plomerová*, 1992; *Babuska et al.*, 1993; *Bormann et al.*, 1996]. The presence of anisotropy will bias isotropic velocity estimates in areas where waves sample predominantly in one direction (usually also areas where smearing occurs and resolution is less). As the direction of anisotropy appears to vary throughout Europe [*Babuska and Plomerová*, 1992; *Babuska et al.*, 1993; *Bormann et al.*, 1996] and P and S waves have different sensitivity and sample the regions differently, anisotropy is not expected to result in a systematic bias on the inversion for temperature. It may, however, result in discrepancies between temperatures derived from P and S velocities in regions where coverage is less than optimal.

3.1. Seismic Velocities

We focus on the lithospheric and sublithospheric mantle under Europe (a tectonic map is shown in Figure 2) for which well-resolved tomographic P and S velocity models are available. The recent P velocity model by *Bijwaard et al.* [1998] and S velocity model by *Marquering and Snieder* [1996] are inverted for temperature.

3.1.1. Velocity models. The compressional velocity model of *Bijwaard et al.* [1998] is a global whole mantle model based on travel times which employs an irregular grid of nonoverlapping cells set up to equalize the ray coverage per cell [*Spakman and Bijwaard*, 1998]. Travel times are from the reprocessed global International Seismological Centre data set of *Engdahl et al.* [1998]. Horizontal resolution in the uppermost mantle under most of continental western Europe is on the scale of the smallest cells, 0.6° to 1.2°. This resolution is similar to that of the regional European-Mediterranean P velocity model of *Spakman et al.* [1993] but with better recovery of the amplitudes of the anomalies in northwestern Europe.

The shear velocity model of *Marquering and Snieder* [1996] (EUR-SC'95) is a regional European model obtained from fitting waveforms in a time window starting at the S wave arrival and ending after the fundamental Rayleigh wave arrival. Using a partitioned waveform inversion which includes the effect of mode coupling [*Marquering et al.*, 1996], a three-dimensional velocity model for the upper mantle is obtained.

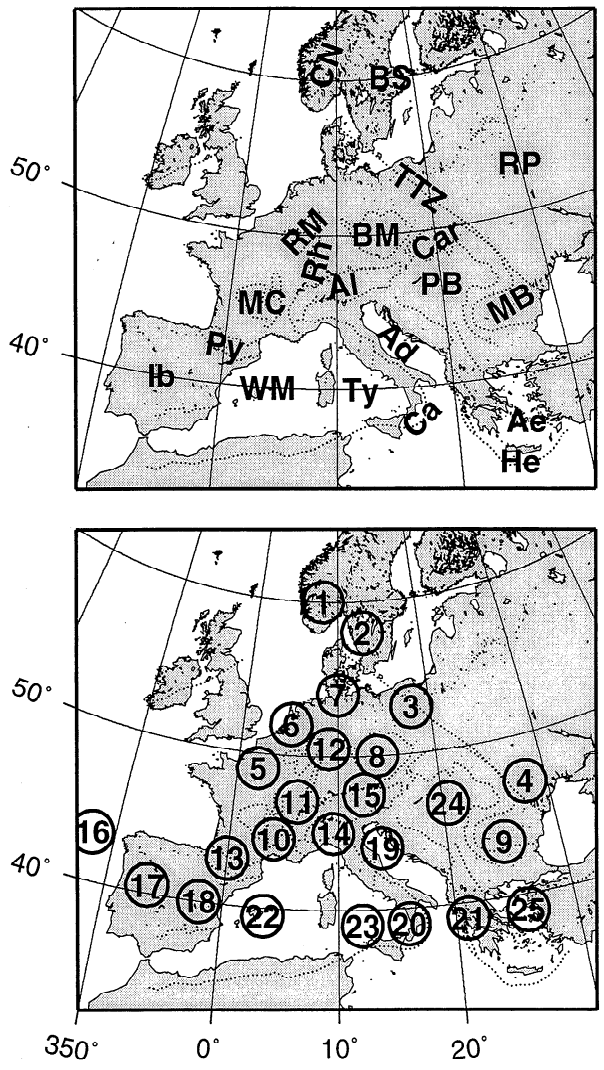

Figure 2. Tectonic map of Europe. CN, Caledonian Norway; BS, Baltic Shield; RP, Russian Platform; RM, Rhenish Massif; Rh, Rhine Graben; BM, Bohemian Massif; MC, Massif Central; Al, Alps; PB, Pannonian Basin; Car, Carpathians; Py, Pyrenees; MB, Moesian Block; Ib, Iberia; WM, Western Mediterranean; Ty, Tyrrhenean Sea; Ca, Calabrian arc; Ad, Adriatic; Ae, Aegean; He, Hellenic arc; TTZ, Tornquist-Teisseyre zone. Numbered circles are the regions where average geotherms and velocity anomalies are determined.

In central Europe, where the ray density is highest, structures on the scale of 0.5° can be recovered [*Marquering and Snieder*, 1996].

A horizontal cross section at 100 km depth through both models is shown in Plate 1. Taking into account the different spatial resolution that is due to the different frequency content of the data used for the P and S velocity models (a representative frequency for the travel time data is 1 Hz, waveforms used in the S wave model contain frequencies up to 60 mHz), both models show similar velocity anomaly patterns, especially in the areas where resolution is thought to be good (i.e., most of continental Europe west of the Tornquist-Teisseyre zone, grossly the area covered by the circles in Figure 2). The difference in spatial resolution is clear in the recovery of the geometry of the small-scale linear slab anomalies under Italy and the Balkans (Plate 1). Note that the amplitude of the shear velocity anomalies is about twice as large as those of the P velocity anomalies.

3.1.2. Correlation V_P and V_S models. A more quantitative comparison of the two models is shown in Figure 3. Twenty-five regions were chosen to cover P and S anomalies associated with different tectonic regimes, with a few additional areas to cover most of the area where resolution of both velocity models is deemed to be good (Figure 2). Anomalies were averaged over circles with a radius of 150 km in order to get a robust estimate. Figure 3 shows the correlation between P and S velocity anomalies at several depths. The error bars represent the standard variation within each circle. Correlation between shear and compressional velocity anomalies is significant at the 95% confidence level at each depth interval. The slope of the lines fit to the data is equal to $\partial \ln V_S / \partial \ln V_P$ or ν. For 100, 150, and 200 km, ν is close to 2 and within the range expected for a purely thermal origin of the anomalies (Table 1). The value of ν decreases slightly between 100 and 200 km depth, but given the standard error of 0.25 on the slope, this decrease cannot be interpreted.

For 55 km depth the slope is larger, which indicates that another effect in addition to temperature plays a role. This may largely be the effect of crustal structure not properly accounted for in the velocity models. The P wave model maps variations in crustal thickness mainly into station corrections and velocity structure in the two crustal layers at 0-15 km and 15-30 km depth [*Bijwaard et al.*, 1998]. The depth of 55 km falls within the first mantle layer of the V_P model. Reference models with different crustal thicknesses were used in the

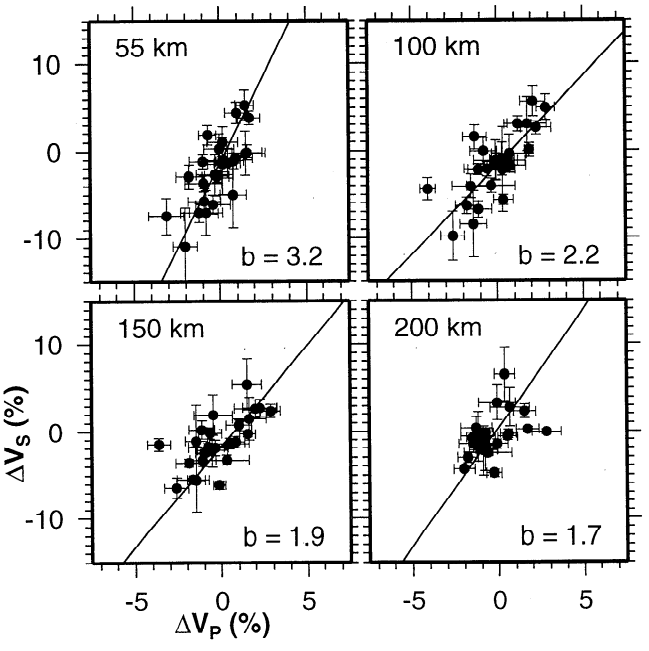

Figure 3. Correlation between P and S velocity anomalies averaged within the circles shown in Figure 2. Error bars represent one standard deviation of the variation within each circle. Lines are a least squares fit to the data. Except at 55 km depth the slopes of the lines (b) are in the range expected for velocity anomalies resulting from thermal structure alone.

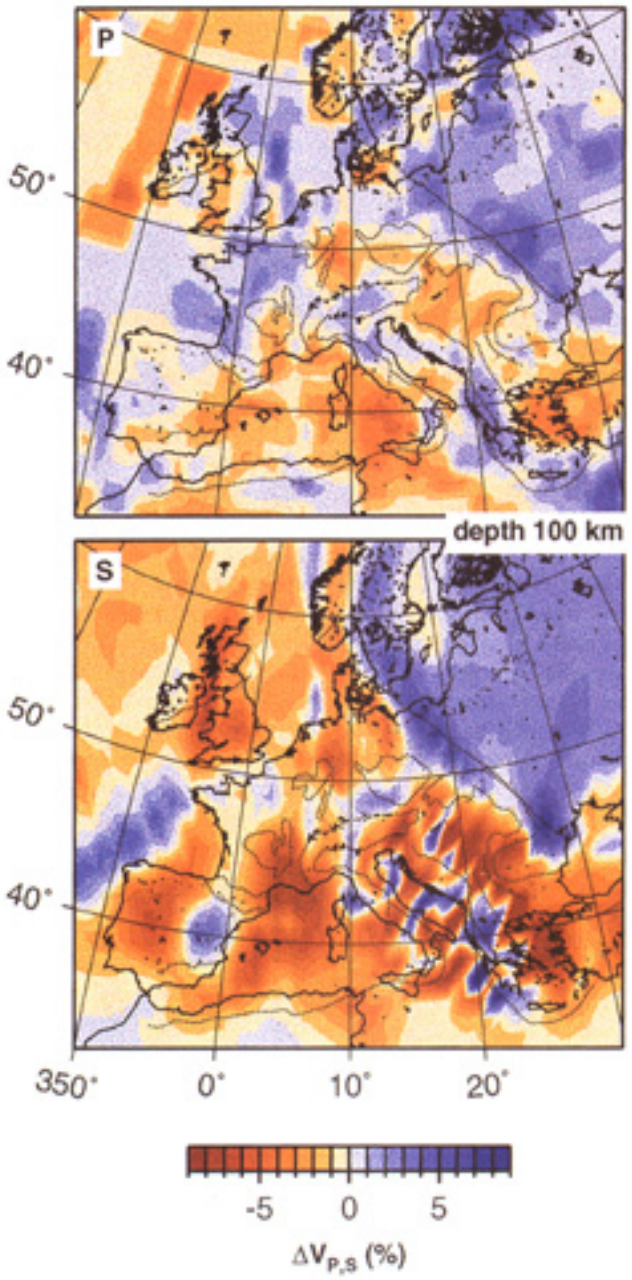

Plate 1. Seismic velocity anomalies at 100 km under Europe. The *P* velocity model is part of the global model from *Bijwaard et al.* [1998], based on the inversion of travel times and using an irregular grid. The *S* wave model is the European model from *Marquering and Snieder* [1996] based on a partitioned waveform inversion which includes mode coupling. *P* anomalies are relative to AK135 [*Kennett et al.*, 1995], *S* anomalies relative to model EUR [*Zielhuis and Nolet*, 1994].

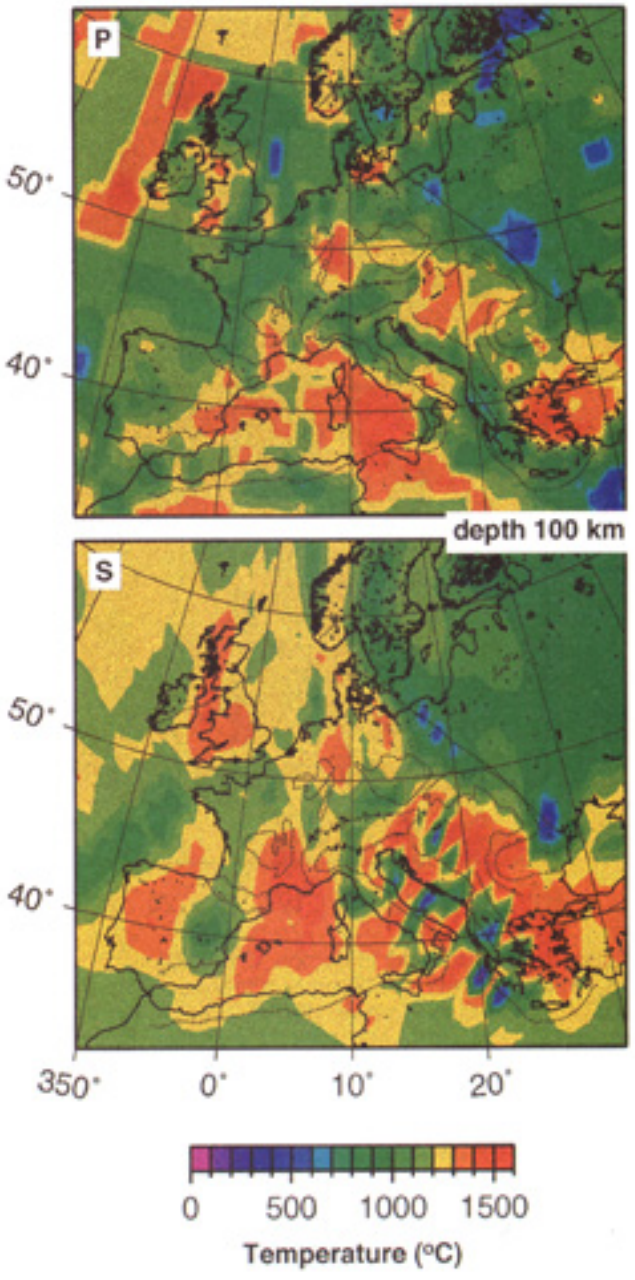

Plate 2. Temperatures at 100 km depth estimated from *P* and *S* velocity anomalies. The composition used is that of a continental garnet lherzolite (acgl [*Jordan*, 1979]) and is assumed to not vary spatially. Anelasticity (Q_1) is taken into account. The assumption that all velocity anomalies can be attributed to variations in temperatures appears to be quite reasonable seeing the similarity in thermal structure obtained from *P* and *S* wave velocities.

inversion for S velocity models along source-receiver paths, but the final three-dimensional model is relative to a reference model with a constant crustal thickness of 29 km [*Marquering and Snieder*, 1996]. This leads to a velocity structure in the upper most layer which mainly reflects incorrect crustal thickness [*Marquering and Snieder*, 1996] and gives low shear velocities for most of continental Europe due to underestimated crustal thickness. V_S at 55 km was obtained by interpolating between velocities at 29 km and the next layer at 80 km depth and is thus also contaminated by crustal structure. We therefore attribute the slope v at 55 km depth mainly to incorrectly modeled crustal structure in the shear velocities, although other factors (such as the presence of water, partial melt, or the mantle phase transition from spinel to garnet lherzolite) may contribute locally.

3.2. Temperatures From Seismic Velocities

3.2.1. Inversion. We do an iterative point by point inversion of seismic velocity for temperature, similar to that by *Furlong et al.* [1995] and *Sobolev et al.* [1997, 1996]. From a given starting temperature we iterate to our final temperature at a given point using the estimated thermal derivatives for the (P,T) conditions and an assumed composition and anelasticity model:

$$T^{n+1} = T^n + F_{\text{damp}}\{ [V_{\text{obs}} - V_{\text{syn}}(T^n)] / [(\partial V/\partial T)_{\text{syn}}(T^n)] \},$$

where T is temperature, n is the iteration number, and V_{obs} and V_{syn} are observed (i.e., tomographic) and synthetic seismic velocity, respectively. Strong damping (factor F_{damp}) is necessary because $\partial V/\partial T$ depends very nonlinearly on temperature due to the effect of anelasticity (see the appendix). Of the order of 50 iterations are necessary to obtain an average difference between observed and synthetic velocity anomalies below 0.1%. We invert absolute velocities (i.e., anomalies plus reference model) and obtain temperatures, not temperature anomalies relative to a reference model. The results are not sensitive to the starting temperature.

The combined inversion of compressional and shear velocity models might give constraints that would allow for a separation of the effects of temperature from those of composition or presence of partial melt [*Furlong et al.*, 1995; *Kennett et al.*, 1998]. Such an approach is, however, not warranted for the velocity models used here. The very different data and imaging techniques used to obtain the two velocity models would result in mapping imaging artifacts into thermal or compositional structure. Instead, P and S velocities were inverted independently. The thermal models are thus subject to the same imaging effects as the individual velocity models, including smearing along rays and uncertainties in the recovery of amplitudes.

3.2.2. Thermal model. The resulting temperatures at 100 km depth are similar for P and S velocities (Plate 2). Lowest temperatures are found east of the Tornquist-Teisseyre zone, which separates the Precambrian shield regions from western Europe. Locally, very high temperatures close to the dry solidus are found under areas with present surface volcanism such as the Massif Central, the Pannonian Basin, and the Aegean. The thermal model shown in Plate 2 uses an average continental garnet lherzolite (acgl) composition [*Jordan*, 1979]. The mean composition of continental garnet lherzolite xenoliths is significantly more depleted (in garnet and clinopyroxene) than average mantle and is probably a representative composition for the continental lithospheric and sublithospheric mantle. At depths shallower than 60-70 km a spinel lherzolite composition would be more appropriate, but as we found composition to have a minor effect on the resulting temperatures (Table 1), a constant composition was used for the whole depth range of 50 to 200 km. The Q model used is Q_1 (Table A2) assuming a frequency of 1 Hz and 0.02 Hz as representative for the waves used for the P and S models, respectively.

3.2.3. Correlation T_P and T_S models. For the numbered regions in Figure 2, temperatures inferred from P (T_P) and S (T_S) velocities are compared in Figure 4. The solid symbols are for the same models using an acgl composition and Q_1 as in the depth slices in Plate 2. The open symbols are for an acgl composition but without a Q model (i.e., $Q \rightarrow \infty$). When no Q is taken into account, the temperatures estimated from V_S are significantly higher than those estimated from V_P. When the Q_1 model is used, the points cluster around the line $T_P = T_S$, except at 55 km depth. The agreement between T_P and T_S is similar for model Q_2, with somewhat lower estimates for the highest temperatures (especially T_S) than when Q_1 is used. This illustrates the importance of including the effect of anelasticity when inverting seismic velocities in the upper mantle for temperature [*Karato*, 1993]. When the effect of Q is included, temperatures obtained from inverting P and S wave velocities agree well. Only at 55 km does thermal structure not seem to be an adequate explanation of both P and S velocity anomalies. We attribute this mainly to not correctly modeled variations in crustal thickness (see section 3.1.2) which will introduce an additional compositional effect due to

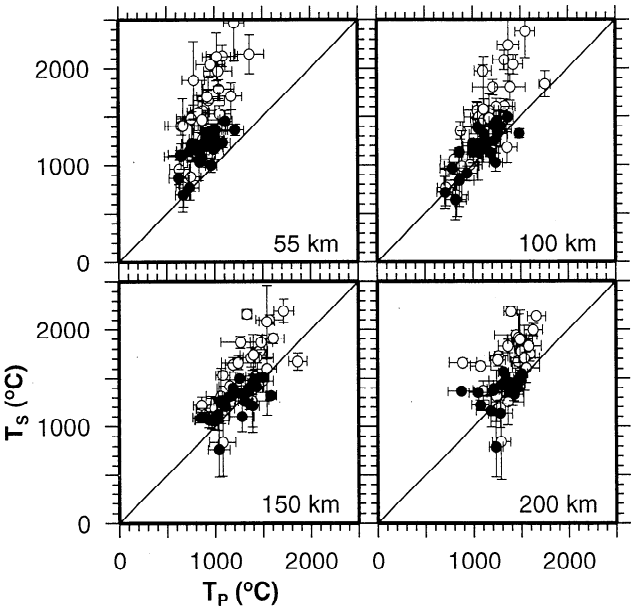

Figure 4. Average temperatures derived from P (T_P) and S (T_S) velocities for the areas shown in the map of Figure 2. Open symbols are temperatures obtained if anelasticity is neglected ($Q \rightarrow \infty$); solid symbols temperatures obtained if model Q_1 is used for the anelasticity. If Q is taken into account, the agreement between temperatures derived from P and S wave velocities is good; the points cluster around the line $T_P = T_S$. At a depth of 55 km, T_S is systematically higher than T_P, probably mainly due to variations in crustal thickness that were not accounted for.

the large difference in crustal and mantle velocities. The general agreement between P and S isotropic velocity patterns (Plate 1) and the inferred thermal structures (Plate 2 and Figure 4) provides additional justification for neglecting anisotropy in a first-order interpretation of seismic structure of the shallow European mantle.

3.3. Comparison With Surface Heat Flow

An independent estimate of temperatures at lithospheric depth can be provided by surface heat flow observations. We compare temperatures estimated from heat flow at 55 km depth with those obtained from P and S velocities. Temperatures from heat flow are estimated by extrapolating along a conductive geotherm. No attempt was made to estimate deeper temperatures from heat flow since the assumption that heat transport is mainly conductive is not valid below the lithosphere. In areas of active volcanism or shallow fluid flow the assumption of conductive heat transport may also not be justified at shallower depths, and thus bias our temperature estimates from heat flow.

Heat flow data are taken from the global heat flow database compiled by *Pollack et al.* [1993]. To smooth some of the variability over short distances that are probably due to very shallow effects and to smooth the very nonuniform coverage, the data are averaged over 1° by 1° blocks. For all of the circled regions in Figure 2, there is at least one (averaged) heat flow value available; most regions contain more heat flow data. In Figure 5 (top) heat flow and velocity data are compared. The correlation between heat flow and seismic velocity anomalies is not as good as between ΔV_P and ΔV_S but is still significant at the 85% confidence level.

To estimate temperatures from heat flow, the one-dimensional continental model from *Chapman* [1986] is used to describe the crustal structure, i.e., the variation of heat production and thermal conductivity with depth. These parameters are not varied laterally. Depth of the Moho and Conrad discontinuities are taken from the CRUST5.1 model [*Mooney et al.*, 1998]. This model gives crustal structure averaged over relatively large regions (5°x5°) compared to the spatial scales in heat flow and tomographic models used here, but as was shown by *Chapman* [1986], the thermal structure at depth is not very sensitive to the depth of these discontinuities. Uncertainties in heat flow measurements and lateral variation in crustal properties have stronger effects on the estimated temperature at depth.

Temperatures estimated from heat flow (q_s) and V_P agree (Figure 5, bottom left), although there is more scatter around the line $T_P = T_{qs}$ than there was for temperatures derived from P and S velocities. Temperatures estimated from shear velocities are systematically higher than those estimated from heat flow (Figure 5, bottom right). This is consistent with our previous inference that the shear velocities at 55 km depth are contaminated more by incorrectly modeled crustal structure than the tomographic P velocities (see section 3.1.2).

4. Temperatures and Tectonics

The agreement between temperature inferred from heat flow and compressional velocities at 55 km and at larger depths between temperatures inferred from V_P and V_S confirms our assumption that seismic velocity anomalies in the shallow mantle under Europe are mainly the result of thermal structure.

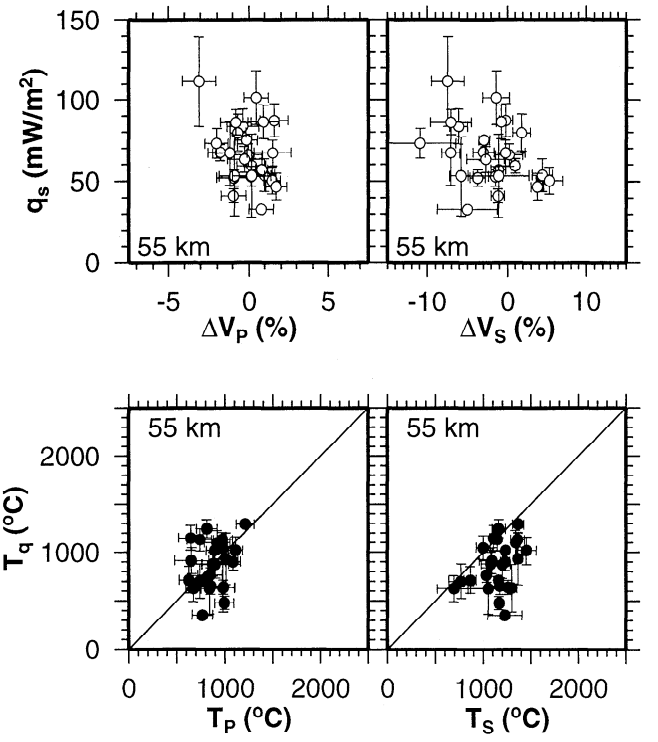

Figure 5. Correlation between (top) heat flow and seismic velocities and (bottom) the temperatures derived from heat flow and from seismic velocities. Heat flow data are taken from the global heat flow database [*Pollack et al.*, 1993] and averaged over 1°x1° squares to smooth the data to a scale similar to that represented by the velocity models. Symbols represent averaged values of 1°x1° heat flow and velocity anomalies over the circles in Figure 2; error bars represent the variation in these circles. Correlation between heat flow and velocity anomalies is not as clear as for V_P and V_S (Plate 2). Temperatures derived from heat flow (extrapolated along steady state conductive geotherms [*Chapman*, 1986]) are consistent with those from V_P (acgl, Q_1, 1 Hz); temperature estimates from V_S (acgl, Q_1, 0.02 Hz) at this depth are probably influenced by variations in crustal thickness.

This gives us some confidence in the thermal structure inferred from the seismic velocities and allows for a closer look at the temperatures found.

4.1. Uncertainty Estimates

For several of the regions in Figure 2 representative of various tectonic regimes the averaged geotherms are shown in Figure 6. Error bars in Figure 6 again indicate the standard deviation around the mean for each circle. The dotted geotherms are an attempt to estimate an uncertainty for the geotherms due to our model parameters. For the heat flow derived geotherms the dotted lines are geotherms with a 20% larger or smaller surface heat flow. This choice was motivated by the uncertainty analysis done by *Chapman* [1986], who showed that uncertainties in surface heat flow measurements have the largest effect on estimated temperatures.

The dotted lines for the velocity-derived geotherms are an estimate of the variation in temperature that would result from the uncertainties in the experimental parameters used for the calculation of anharmonic velocity (the appendix, Table A1).

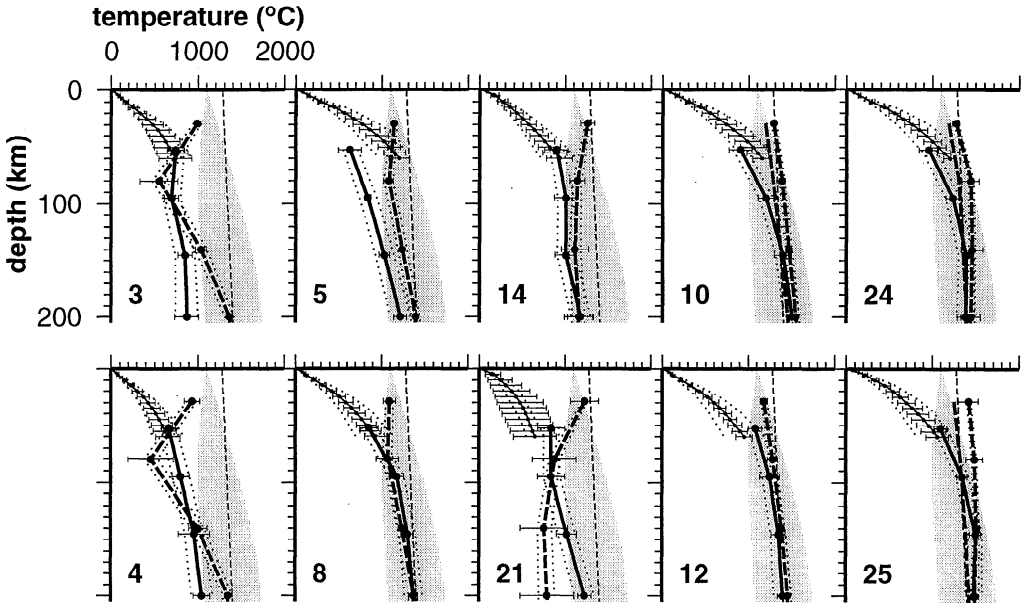

Figure 6. Selected geotherms from the areas in Figure 2 inferred from V_P (acgl, Q_1, 1 Hz, bold solid lines with symbols), V_S (acgl, Q_1, 0.02 Hz, bold dashed lines with symbols), and heat flow (thin solid lines with symbols). Dotted lines illustrate estimated uncertainty: for $V_{P,S}$ due to uncertainties in the experimental parameters used and for heat flow using heat flow values that are ± 20% of the observed heat flow. Error bars illustrate the spread within the circles. For the hottest regions (10, 24, 25) an extra T_S geotherm is shown using Q_2 (bold dashed line without symbols). For reference, the area between the wet and dry mantle solidi (shaded) [*Thompson*, 1992] and the mantle adiabat (potential temperature 1280°C, thin dashed line) are shown.

Temperatures derived using Q_2 instead of Q_1 usually fall within these uncertainty bounds. Where this is not the case (for S velocities in the regions with the highest temperatures where the effect of Q is strongest), Q_2 geotherms are also shown. Increasing all velocity anomalies by 20% to account for the uncertainty in the amplitude of the tomographic anomalies, which may be underestimated due to the damping applied in the tomographic inversion, generally gives temperature variations that again fall within the uncertainty bounds estimated from the experimental uncertainties. The largest changes in temperature due to the 20% stronger anomalies are in the coldest regions.

In summary, *Chapman* [1986] estimates the uncertainty in heat flow derived temperatures to be 100-200°C at Moho depths. We estimate the uncertainties in the temperatures derived from the seismic velocities to be ~100-150°C, with larger uncertainties associated with the extrapolation of experimental parameters to larger temperatures and pressures.

4.2. Regional Geotherms

4.2.1. Shields. Two shield geotherms from regions 3 and 4 located just east of the Tornquist-Teisseyre zone (TTZ) are shown in Figure 6. Surface heat flow and V_P-derived geotherms seem to agree well for these two regions and indicate very low temperatures, only 900-1000°C at 200 km depth, relative to "normal" mantle (represented by an adiabat with a potential temperature of 1280°C [*McKenzie and Bickle*, 1988]). Temperatures estimated from S velocities do not agree with the heat flow-V_P geotherm. At shallow depths this can be attributed to the large crustal thickness under the Russian platform [*Meissner et al.*, 1987; *Mooney et al.*, 1998] which results in relatively low velocities just below 29 km which are translated into relatively high temperatures. At 150-200 km depth, S waves may already be influenced by the low shear velocity anomaly that *Nolet and Zielhuis* [1994] identified at depths between 300 and 500 km east of the TTZ. If present, the additional effect of a relatively depleted composition for shield areas [*Griffin et al.*, 1999, 1998; *Jordan*, 1988] would result in a lower estimate of T_S than T_P (as seen around 80 km depth, Figure 6). However, in addition to the above mentioned uncertainties in S wave velocities, the resolution of the P velocities also deteriorates east of the TTZ. Thus the resolution of these tomographic models in the shield areas does not really allow us to evaluate whether a compositional effect is present in the velocities.

4.2.2. Tectonically relatively quiet western Europe. Region 5 (western France) has been a tectonically relatively quiet region since the Hercynian orogeny. Heat flow in this area is probably influenced by hydrothermal circulation in the thick sediments of the Parisian basin. Under the Netherlands (region 6), P and S geotherms are very similar to those of region 5. The few available heat flow data for region 6, however, give temperatures quite consistent with T_P. The reason for the discrepancy between T_P and T_S for these regions may be a less than optimal resolution and amplitude recovery of the velocity anomalies as they are located at the edge of the region where resolution is good. In any case the temperatures here are higher than under the Russian Platform and are probably the closest to an estimate of an undisturbed Hercynian geotherm.

The geotherm under the Bohemian Massif (region 8) can be compared to the geotherm of region 3 to get an estimate of the

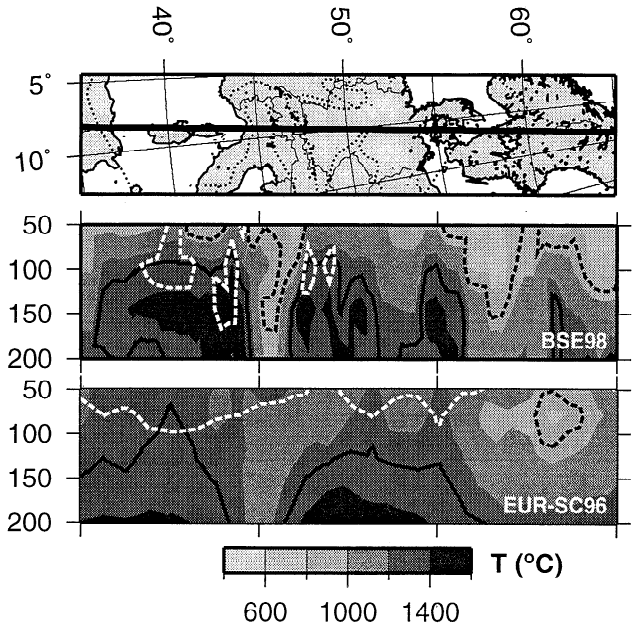

Figure 7. Temperatures from P and S wave velocity along the trend of the European Geotraverse between 50 and 200 km depth. Bold solid line marks the bottom of the thermal lithosphere, assuming it corresponds with the 1300°C isotherm. The bottom of the mechanical lithosphere (solid dashed line) is identified with a strength of 1 MPa assuming a dry olivine rheology [*Kirby*, 1983]. The area where *Hirth and Kohlstedt*'s [1996] solidus is crossed is indicated by the white dashed contours. Dry melting is not expected anywhere along the profile.

contrast in temperature across the TTZ. This contrast is ~300°C and may be slightly higher farther south where the Pannonian Basin (region 25) is located west of the TTZ. Temperatures under the Bohemian Massif from V_P, V_S, and heat flow agree well (T_S at 29 km may be biased by the presence of thickened crust). The temperatures under the Bohemian Massif may be influenced by the high-temperature anomaly to the west, which has been related to the Eifel volcanism [*Hoernle et al.*, 1995; *Zeyen et al.*, 1997].

4.2.3. Subduction zones. Two geotherms for subduction zones, under the Hellenic arc (region 21) and under the western Alps (region 14) are shown in Figure 6. Although both P and S waves image high-velocity anomalies in the regions, the structure is too narrow to image the geometry well using the longer-wavelength surface waves. This can probably explain the discrepancy between T_P and T_S for the Hellenic slab, and the large error bars reflect the effect of averaging over the dipping slab. Temperatures in this subduction zone may be as low as 700°C at ~150 km depth. Such low temperatures are in agreement with kinematic thermal models for subduction zones [e.g., *de Jonge et al.*, 1994]. Convergence in the western Alps occurs at a slow rate and probably involves some subduction of continental material. Temperatures indicate a warmer slab and probably some effect of the thickened crust on T_S.

4.2.4. Plumes. The Massif Central (region 10) and the Rhenish Massif/Eifel (region 12) are regions with recent volcanism where the presence of a plume or several small plumes have been proposed [*Hoernle et al.*, 1995; *Sobolev et al.*, 1997; *Zeyen et al.*, 1997]. Elevated temperatures, close to the 1280°C mantle adiabat up to depths as shallow as 100 km under the Massif Central and even shallower under the Rhenish Massif, are indeed found for both regions. Under the Eifel, T_P and T_S agree well, thus not showing any indication for the presence of melt. P velocities, which may resolve small-scale structure better, locally give temperatures which reach the dry solidus (Plate 2), so on a small scale, melt may be present but not enough to significantly affect the seismic velocities. The high temperatures at shallow depths under the Eifel are similar to an "alkaline province" geotherm derived from xenoliths from various continental rift areas [*Jones et al.*, 1983]. Under the Massif Central where the crust is <25 km thick [*Meissner et al.*, 1987], the divergence of T_P and T_S at depths <100 km could indicate the presence of melt. If the mantle is not completely dry, for example, using estimates for the water content of the mantle of [*Hirth and Kohlstedt*, 1996], temperatures reach the solidus at these shallow depths. The geotherm under the Massif Central is consistent with the more detailed thermal structure for this area from [*Sobolev et al.*, 1997, 1996]. *Sobolev et al.* [1997] infer small amounts of melt (temperatures above the dry solidus) from a local P wave model. Our use of P and S waves may provide an indication of the presence of melt even with much coarser spatial resolution.

4.2.5. Back-arc extensional areas. The highest temperatures are found for areas that currently are or have been under extension, for example, the Pannonian Basin (region 24) and the Aegean (25). Similar geotherms are found for the Tyrrhenian Sea (region 22) and the western Mediterranean (region 23). Temperatures are close to the mantle adiabat up to depths as shallow as 100 km. Above 100 km depth, differences between T_P and T_S could again be indicative for the presence of some melt, noting that crustal thickness in these regions is less than average due to stretching. The position of the zones behind retreating subduction zones makes melting enhanced by the presence of water plausible.

4.3. Temperatures Along the EGT

In Figure 7 we show a cross section approximately paralleling the European Geotraverse (EGT). The EGT project was an interdisciplinary effort to increase understanding of the structure and properties of the European continental crust and lithosphere [*Blundell et al.*, 1992] Running from northern Norway to the tip of northern Africa the EGT crosses various tectonic regions. The temperatures can be compared with the three-dimensional thermal model along the EGT derived by *Cermák and Bodri* [1995] from a contour map of European surface heat flow [*Cermák and Hurtig*, 1979; *Cermák and Rybach*, 1979] using a model which includes conduction in three dimensions.

Note the high temperatures at shallow depths under the western Mediterranean and under central Germany (Figure 7), possibly even high enough for some melt. The white dashed contours outline the area where temperatures are above the solidus based on *Hirth and Kohlstedt*'s [1996] estimate of a reasonable water content for the uppermost mantle. The shallow region of melt in the S model is probably overestimated, as temperatures at these depths are probably overestimated (Figures 4 and 5). Nowhere along the profile do the temperatures cross the dry solidus.

The profile in Figure 7 crosses the southward subducting slab under the Alps and the western end of the Tornquist-

Teisseyre zone. At 50 km depth, *Cermák and Bodri* [1995] find temperatures <600°C under the Baltic Shield, temperatures >1050°C northwest of the Alps and under the Tyrrhenean Sea, and steep thermal gradients to a minimum temperature of 500-600°C under the western Alps. This agrees well with the temperatures at this depth inferred from *P* waves (Figure 7). Not consistent are our relatively high temperatures under Caledonian Norway (this is clearer in Plate 2). T_P is around 1000°C at 50 km depth under southern Norway, where low surface heat flow gives temperatures <650°C [*Cermák and Bodri*, 1995]. At larger depths, both T_P and T_S show a contrast between relatively warm temperatures under Norway and low temperatures under the Swedish part of the Baltic Shield (Plate 2).

4.4. Lithospheric Thickness

The thermal models derived from seismic velocities can be used to estimate temperature-dependent properties, for example, the rheology or thickness of the lithosphere. From both T_P and T_S, thermal and mechanical thickness of the lithosphere were estimated (Figure 7). The estimated thermal thickness of the lithosphere defined as the depth of the 1300°C isotherm ranges from >200 km under the Russian platform to around 50-60 km locally under the Eifel, Massif Central, and the extensional Pannonian, Aegean, western Mediterranean, and Tyrrhenean Basins. Under the westernmost part of continental Europe, lithospheric thickness estimates range from 150 km based on V_S to 200 km based on V_P. Our estimated thermal thickness of the lithosphere is very similar to the seismic lithospheric thickness estimated by *Babuska and Plomerová* [1992] . They map *P* wave travel time residuals from teleseismic and regional data into variations in lithospheric thickness under the assumption that the seismic lithosphere is a high-velocity layer overlying the low-velocity asthenosphere. The thickness of the lithosphere based on surface wave modeling [*Panza*, 1985; *Panza et al.*, 1980] is slightly thinner but displays similar patterns as our thermal thickness, taking into account the coarser resolution of the surface wave image. The surface wave based lithospheric thickness agrees with the thermal thickness inferred from heat flow data by *Cermák and Bodri* [1995], who used a different definition of the thermal lithosphere which corresponds to lower limiting temperatures.

The mechanical thickness of the lithosphere when defined as the depth of the 10 MPa strength contour [*Ranalli*, 1994] is significantly thinner than the thermal lithosphere. The lithospheric strength was calculated using the rheology for dry olivine from *Kirby* [1983]. This yields mechanical thicknesses of a maximum of 150 km under the Baltic Shield to <50 km under the Tyrrhenean Basin and central Europe (Figure 7). If the definition for mechanical thickness from *Cloetingh and Burov* [1996] is used, somewhat smaller mechanical thicknesses are found, from 100-125 km under the shield areas to <50 km (only temperatures inferred from seismic velocities were used, which does not give any constraints at depths above 50 km) under most of the rest of Europe.

5. Conclusions

Lateral variations in seismic velocities as mapped using seismic tomography are usually interpreted in terms of thermal structure. Previous work has shown that the effect of thermal variations on seismic velocities in the uppermost mantle is probably considerably larger than the effect of reasonable variations in composition [*Jackson and Rigden*, 1998; *Jordan*, 1979; *Sobolev et al.*, 1996]. Synthetic velocity calculations for one-dimensional thermal models at depths between 50 and 200 km based on experimentally determined parameters predicts a 0.5 to 2% decrease in *P* wave velocity for a 100°C increase in temperature. For *S* waves the decrease in velocity would be between 0.7 and 4.5% for a 100°C increase in temperature. The largest changes are for high temperatures where anelasticity has an important influence. In contrast, variations in composition inferred from mantle xenoliths usually do not give changes in velocity larger than 1%. This does not mean that variations in composition are not important. The effect on density is potentially large [*Griffin et al.*, 1999, 1998; *Jordan*, 1988] and of geodynamic importance [*Jordan*, 1988]. The effect of the presence of partial melt is probably large [*Sato et al.*, 1989; *Schmeling*, 1985] but strongly dependent on the geometry of the melt pockets [e.g., *Schmeling*, 1985].

On the basis of the sensitivity analysis we set up a procedure to invert seismic velocity anomalies in the shallow mantle (50-200 km depth) for temperatures. We applied the inversion to two high-quality tomographic models under Europe, the *P* wave model based on travel times from *Bijwaard et al.* [1998] and the *S* wave model based on waveform modeling from *Marquering and Snieder* [1996]. Except at the level just below the crust the ratio of *S* to *P* velocity anomalies is consistent with a predominant thermal origin of the anomalies. Temperatures inferred from *P* and *S* velocities at depths larger than 80 km agree well with each other. Furthermore, the temperatures obtained from the *P* wave model are consistent with temperatures at 55 km depth estimated from surface heat flow observations [*Pollack et al.*, 1993]. *S* wave derived temperatures at this depth are consistently higher than those estimated from *P* wave velocity or heat flow and probably mainly reflect the compositional effect of thickened crust. In the warmest areas, subcrustal T_S may also be influenced by the presence of melt and/or water. Anisotropy is an unlikely explanation for the consistent offset between subcrustal T_P and T_S over the different regions. Uncertainties in the temperatures are estimated to be ~100-150°C. Testing of the effects of the applied tomographic imaging procedures is necessary to further understand discrepancies found between *P* and *S* wave derived thermal structure.

The lateral variation in temperature of up to 1000°C that we obtain using experimental anelasticity models is accompanied by a large lateral variation in anelasticity from values <50 in the hottest areas to values that are effectively infinite in the coldest areas. Regional tomographic Q modeling could test this result.

The thermal structure obtained from the seismic velocity models is consistent with surface tectonics. Temperatures below the Russian Platform are estimated to be ~400°C below an average mantle adiabat at 200 km depth. The thermal contrast across the Tornquist-Teisseyre zone which separates Hercynian Europe from the Precambrian shields to the east is ~300°C. High temperatures, close to the mantle adiabat, and a thermal lithospheric thickness of only 50-60 km are found under the Massif Central and the Rhenish Massif, where the presence of a plume(s) has been proposed [*Hoernle et al.*, 1995; *Zeyen et al.*, 1997]. The highest temperatures were

imaged under the extensional Pannonian, western Mediterranean, Tyrrhenean, and Aegean Basins. As temperatures in the regions approach the dry solidus and crustal thickness is lower than average in these regions, the discrepancy between temperatures inferred from P and S waves may be due to the presence of partial melt. At depths larger than ~100 km, temperatures are generally below the solidus based on *Hirth and Kohlstedt*'s [1996] estimate of the water content of the mantle.

On the basis of this analysis we conclude that in areas where the resolution of tomographic models is good, compressional and shear wave velocities can be mapped into thermal structure. While uncertainties in the tomographic models and in the experimental parameters used may not allow us to resolve any effects other than thermal with the possible exception of the presence of partial melt, these temperature estimates are useful to get further insight in the rheology and dynamics of the shallow mantle.

Appendix

A1. Anharmonicity

For shallow depths (pressures up to about 6 GPa), density ρ, compressibility K, and rigidity μ can be computed at a given (P,T) condition from their values at the reference state (P_0,T_0) using the infinitesimal strain approximation:

$$M(P,T) = M(P_0,T_0) + (T-T_0)\frac{\partial M}{\partial T} + (P-P_0)\frac{\partial M}{\partial P}, \qquad \text{(A1)}$$

where M stands for either of the elastic parameters K or μ. For density the equation can be simplified using the definitions of α (thermal expansion) and K:

$$\rho(P,T) = \rho(P_0,T_0)\,[1- \alpha_0(T-T_0) + \frac{(P-P_0)}{K}]\,. \qquad \text{(A2)}$$

The Voigt-Reuss-Hill (VRH) averaging scheme approximates the parameters for a combination of minerals by taking the average of the mean elastic parameters for a constant stress (Reuss) and a constant strain (Voigt) situation:

$$\langle\rho\rangle = \Sigma\lambda_i\rho_i \qquad \text{(A3a)}$$

$$\langle M\rangle = \frac{1}{2}\left(M^{\text{voigt}} + M^{\text{reuss}}\right);$$

$$M^{\text{voigt}} = \Sigma\lambda_i M_i\ ;\ M^{\text{reuss}} = \left(\Sigma\frac{\lambda_i}{M_i}\right)^{-1}, \qquad \text{(A3b)}$$

where λ_i is the volumetric proportion of mineral i.

To calculate partial derivatives of seismic velocity V, the equations for the VRH averaging scheme were differentiated giving the following expressions:

$$\frac{\partial V}{\partial \xi} = \left[\frac{\partial\langle M\rangle}{\partial \xi} - V^2\frac{\partial\langle\rho\rangle}{\partial \xi}\right] / \left[2\langle\rho\rangle V\right], \qquad \text{(A4)}$$

where $<\rho>$ and $<M>$ are the VRH-averaged properties, M now is equal to $K+4\mu/3$ for P waves or equal to μ for S waves. The parameter ξ can be, for example, temperature, iron content, or amount of partial melt:

$$\frac{\partial\langle\rho\rangle}{\partial \xi} = \Sigma\lambda_i\frac{\partial\rho_i}{\partial \xi} \qquad \text{(A5a)}$$

$$\frac{\partial\langle M\rangle}{\partial \xi} = \Sigma\lambda_i\frac{\partial M_i}{\partial \xi} + \left(M^{\text{reuss}}\right)^2\Sigma\frac{\lambda_i}{M_i^2}\frac{\partial M_i}{\partial \xi}. \qquad \text{(A5b)}$$

The values for density and the elastic parameters and their derivatives used in this paper are given in Table A1.

Table A1. Elastic Parameters

Mineral	Unit	Olivine Mg_2SiO_4	Orthopyroxene $MgSiO_3$	Clinopyroxene $CaMgSi_2O_6$	Spinel $MgAl_2O_4$	Garnet $Mg_3Al_2Si_3O_{12}$
ρ	10^{-3} kg/m^3	3.222[a] (2)[a]	3.198[b](5)[a]	3.280[c] (5)[a]	3.578[d] (5)[e]	3.565[f] (5)[g]
$d\rho/dX_{Fe}$		1.182[a] (5)[g]	0.804[h,i] (5)[a]	0.377[c,j] (5)[a,g]	0.702[d,k] (5)[g]	0.758[f] (5)[g]
K_S	GPa	129[l] (1)[m,g]	111[h,i] (2)[a,h]	105[n] (1)[n]	198[d] (5)[e]	173[f] (2)[f]
$\partial K_S/\partial X_{Fe}$		0[a] (1)[g,p]	-10[h,i] (2)[g]	13[n] (2)[g]	12[d,k] (4)[g]	7[f] (2)[g]
μ	GPa	82[p](2)[p]	81[h,i] (2)[a,g,h]	67[c] (2)[a]	108[d] (3)[e]	92[f] (1)[f]
$\partial\mu/\partial X_{Fe}$		-30[p] (1)[a]	-29[h,i] (3)[g]	-6[c,j] (2)[g]	-24[d,k] (4)[g]	7[f] (2)[g]
K_S'		4.2[l] (2)[l]	6.0[h] (5)[g,h]	6.2[n] (3)[n]	5.7[d] (8)[g]	4.9[f] (5)[f]
$\partial K_S'/\partial X_{Fe}$				-1.9[n] (4)[n]		
μ'		1.4[l] (1)[l]	2.0[h] (1)[h]	1.7[a] (2)[g]	0.8[q] (5)[g]	1.4[f] (1)[f]
$\partial K_S/\partial T$	MPa/K	-16[p,r] (2)[g,p,r]	-12[a] (3)[g]	-13[a] (3)[g]	-28[c] (5)[g]	-21[f] (2)[f]
$\partial\mu/\partial T$	MPa/K	-14[p] (1)[a]	-11[a] (2)[g]	-10[a] (2)[g]	-12[c] (3)[g]	-10[f] (1)[f]
α_0	10^{-4} K^{-1}	0.2010[s]	0.3871[s]	0.3206[s]	0.6969[s]	0.0991[s]
α_1	10^{-7} K^{-2}	0.1390[s]	0.0446[s]	0.0811[s]	-0.0108[s]	0.1165[s]
α_2	10^{-2}	0.1627[s]	0.0343[s]	0.1347[s]	-3.0799[s]	1.0624[s]
α_3	K	-0.3380[s]	-1.7278[s]	-1.8167[s]	5.0395[s]	-2.5000[s]

Error estimates in the last digit are given in parentheses. These are either taken directly from the literature or, if not available, are estimated from comparison of the values given by different authors or from uncertainties for other minerals.

[a] *Duffy and Anderson* [1989].
[b] *Weidner et al.* [1978].
[c] *Levien et al.* [1979].
[d] *Yoneda* [1990].
[e] *Anderson and Isaak* [1995].
[f] *Chen et al.* [1997].
[g] Estimated.
[h] *Webb and Jackson* [1993].
[i] *Bass* [1984].
[j] *Kandelin and Weidner* [1988].
[k] *Wang and Simmons* [1972].
[l] *Zha et al.* [1996].
[m] *Duffy et al.* [1995].
[n] *Zhang et al.* [1997].
[p] *Isaak* [1992].
[q] *Anderson et al.* [1968].
[r] *Meng et al* [1993].
[s] *Saxena and Shen*, 1992]; uncertainty in a is estimated to be 20%

Table A2. Anelasticity Parameters

	a	A	H^*, kJ/mol	V^*, cm^3/mol
Q_1	0.15	1.48×10^{-1}	500	20
Q_2	0.25	2.0×10^{-4}	584	21

Q_1 is after *Sobolev et al.* [1996]. Their Q model 2 based on average experimental data for α, H^*, and V^* with A calibrated to fit seismic observations. Q_2 is after *Berckhemer et al.* [1982] from experimental data for forsterite. V^* is estimated from the relation used by *Kampfmann and Berckhemer* [1985]: $V^*/H^* = 33 \times 10^{-3}$ GPa^{-1}.

A2. Anelasticity

It is generally assumed that the main anelasticity effect Q is associated with the shear modulus μ:

$$Q_\mu = A\omega^a \exp(aE^*/RT), \quad E^* = H^* + PV^*, \tag{A6}$$

where A is a constant, H^* is activation energy, V^* is activation volume, and P and T denote pressure and temperature, respectively. The parameter ω is frequency, and a is the frequency exponent which is assumed to be small for seismic waves ($0<a<1$). $Q_S = Q_\mu$ and Q for P waves is given by [e.g., *Anderson and Given*, 1982]:

$$Q_P^{-1} = (1-L)Q_K^{-1} + LQ_\mu^{-1}, \tag{A7}$$

where $L = (4/3)(V_S/V_P)^2$ and Q_K is generally taken to be a constant, usually $\rightarrow \infty$

Velocity taking into account both anharmonic and anelastic effects for weakly frequency dependent Q can be expressed as follows [*Minster and Anderson*, 1981] :

$$V(P,T,X,\omega) = V_{anh}(P,T,X)\left[1 - \frac{2Q^{-1}(\omega,T)}{\tan(\pi a/2)}\right], \tag{A8}$$

where X stands for composition. $(\partial V/\partial T)_{anel}$ for $Q^{-1} << 1$ becomes [see also, *Karato*, 1993]

$$\left(\frac{\partial V}{\partial T}\right)_{anel} = Q^{-1}(\omega,T)\frac{aH^*}{2RT^2\tan(\pi a/2)}, \tag{A9}$$

The complete temperature derivatives are given by $\partial V/\partial T = (\partial V/\partial T)_{anh} + (\partial V/\partial T)_{anel}$, where $(\partial V/\partial T)_{anh}$ is calculated using (A4) and $(\partial V/\partial T)_{anel}$ is calculated using (A9). The values used for the anelasticity parameters can be found in Table A2.

Acknowledgments. First and foremost, we thank Harmen Bijwaard, Wim Spakman, and Roel Snieder for the use of their velocity models which made this study possible and for discussions on the interpretation and shortcomings of the models. Discussions with Martin Drury, Axel Röhm, Mark Rehkämper, and Eveline Rosendaal helped to shape the project. The exploratory calculations of synthetic velocities for the Mendocino Triple Junction area, which Ian Dillisse performed for his master's thesis, provided a starting point for the research presented here. We also thank S. O'Reilly, M. Bostock, and an anonymous reviewer for their helpful and constructive reviews. All figures were made using GMT3.0 [*Wessel and Smith*, 1995]. This is a contribution to the NEESDI (Netherlands Environmental Earth System Dynamics Initiative) programme, partly funded by the Netherlands Organization for Scientific Research (NWO grant 750-29-601). A contribution of the Vening-Meinesz Research School of Geodynamics.

References

Anderson, D.L., and J.W. Given, Absorption band Q model for the Earth, *J. Geophys. Res.*, *87*, 3893-3904, 1982.

Anderson, D.L., and R.S. Hart, Attenuation models of the Earth, *Phys. Earth Planet. Inter.*, *16*, 289-306, 1978.

Anderson, O.L., and D.G. Isaak, Elastic constants of mantle minerals at high temperature, in *Mineral Physics and Crystallography: A Handbook of Physical Constants, AGU Ref. Shelf*, vol. 2, edited by T.J. Ahrens, pp. 64-97, AGU, Washington, D.C., 1995.

Anderson, O.L., E. Schreiber, and R.C. Liebermann, Some elastic constant data on minerals relevant to geophysics, *Rev. Geophys.*, *6*, 491-495, 1968.

Babuska, V., and J. Plomerová, The lithosphere in central Europe-Seismological and petrological aspects, *Tectonophysics*, *207*, 141-163, 1992.

Babuska, V., J. Plomerová, and J. Síleny, Models of seismic anisotropy in the deep lithosphere, *Phys. Earth Planet. Inter.*, *78*, 167-191, 1993.

Bass, J.D., Elasticity of single crystal ferrosilite, *J. Geophys. Res.*, *89*, 4359-4371, 1984.

Bass, J.D., Elasticity of minerals, glasses, and melts, in *Mineral Physics and Crystallography: A Handbook of Physical Constants, AGU Ref. Shelf*, vol. 2, edited by T.J. Ahrens, pp. 45-63, AGU, Washington D.C., 1995.

Berckhemer, H., W. Kampfman, E. Aulbach , and H. Schmeling, Shear modulus and Q of forsterite and dunite near partial melting from forced oscillation experiments, *Phys. Earth Planet. Inter.*, *29*, 30-41, 1982.

Bijwaard, H., W. Spakman, and E.R. Engdahl, Closing the gap between regional and global travel time tomography, *J. Geophys. Res.*, *103*, 30,055-30,078, 1998.

Blundell, D., R. Freeman, and S. Mueller, *A Continent Revealed: The European Geotraverse*, 275 pp., Cambridge Univ. Press, New York, 1992.

Bormann, P., G. Grünthal, R. Kind, and H. Montag, Upper mantle anisotropy beneath Central Europe from *SKS* wave splitting: Effects of absolute plate motion and lithosphere-asthenosphere boundary topography?, *J. Geodyn.*, *22*, 11-32, 1996.

Cermák, V., and L. Bodri, Three-dimensional deep temperature modelling along the European geotraverse, *Tectonophysics*, *244*, 1-11, 1995.

Cermák, V., and E. Hurtig (Eds.), Heat flow map of Europe, scale 1:5,000,000, in *Terrestrial Heat Flow in Europe*, edited by V. Cermák, and L. Rybach, Springer-Verlag, New York, 1979.

Cermák, V., and L. Rybach (Eds.), *Terrestrial Heat Flow in Europe*, 329 pp., Springer-Verlag, New York, 1979.

Chapman, D.S., Thermal gradients in the continental crust, in *The Nature of the Lower Continental Crust*, edited by J.B. Dawson et al., pp. 63-70, Geol. Soc. London, 1986.

Chen, G., R. Miletich, K. Mueller, and H.A. Spetzler, Shear and compressional mode measurements with GHz ultrasonic interferometry and velocity-composition systematics for pyrope-almandine solid solution series, *Phys. Earth Planet. Inter.*, *99*, 273-287, 1997.

Cloetingh, S., and E.B. Burov, Thermomechanical structure of European continental lithosphere: Constraints from rheological profiles and EET estimates, *Geophys. J. Int.*, *124*, 695-732, 1996.

de Jonge, M.R., M.J.R. Wortel, and W. Spakman, Regional scale tectonic evolution and the seismic velocity structure of the lithosphere and upper mantle: The Mediterranean region, *J. Geophys. Res.*, *99*, 12,091-12,108, 1994.

Der, Z.A., A.C. Lees, and V.F. Cormier, Frequency dependence of Q in the mantle underlying the shield areas of Eurasia, part III, The Q model, *Geophys. J. R. Astron. Soc.*, *87*, 1103-1112, 1986.

Duffy, T.S., and D.L. Anderson, Seismic velocities in mantle minerals and the mineralogy of the upper mantle, *J. Geophys. Res.*, *94*, 1895-1912, 1989.

Duffy, T.S., C. Zha, R.T. Downs, H. Mao, and R.J. Hemley, Elasticity of forsterite to 16 GPa and the composition of the upper mantle, *Nature*, *378*, 170-131, 1995.

Durek, J.J., and G. Ekström, A radial model of anelasticity consistent with long-period surface-wave attenuation, *Bull. Seismol. Soc. Am.*, *86*, 144-158, 1996.

Engdahl, E.R., R.D. van der Hilst, and R.P. Buland, Global teleseismic earthquake relocation with improved travel times and procedures for depth determination, *Bull. Seismol. Soc. Am.*, *88*, 722-743, 1998.

Faul, U.H., D.R. Toomey, and H.S. Waff, Intergranular basaltic melt is distributed in thin, elongated inclusions, *Geophys. Res. Lett.*, *21*, 29-32, 1994.

Forte, A.M., R.L. Woodward, and A.M. Dziewonski, Joint inversions of

seismic and geodynamic data for models of three-dimensional mantle heterogeneity, *J. Geophys. Res.*, *99*, 21,857-21,887, 1994.

Forte, A.M., A.M. Dziewonski, and R.J. O'Connell, Thermal and chemical heterogeneity in the mantle: A seismic and geodynamic study of continental roots, *Phys. Earth Planet. Inter.*, *92*, 45-55, 1995.

Furlong, K.P., W. Spakman, and M.J.R. Wortel, Thermal structure of the continental lithosphere: Constraints from seismic tomography, *Tectonophysics*, *224*, 107-117, 1995.

Griffin, W.L., S.Y. O'Reilly, C.G. Ryan, O. Gaul, and D.A. Ionov, Secular variation in the composition of subcontinental lithospheric mantle: Geophysical and geodynamic implications, in *Structure and Evolution of the Australian Continent*, *Geodyn. Ser.*, vol. 26, edited by J. Braun et al., pp. 1-26, AGU, Washington, D.C., 1998.

Griffin, W.L., S.Y. O'Reilly, and C.G. Ryan, The composition and origin of sub-continental lithospheric mantle, in *Mantle Petrology: Field Observations and High-Pressure Experimentation*, edited by Y. Fei, Geochem. Soc., USA, in press, 1999.

Hirth, G., and D.L. Kohlstedt, Water in the oceanic upper mantle: Implications for rheology, melt extraction and the evolution of the lithosphere, *Earth Planet. Sci. Lett.*, *144*, 93-108, 1996.

Hoernle, K., Y. Zhang, and D. Graham, Seismic and geochemical evidence for large-scale mantle upwelling beneath the eastern Atlantic and western and central Europe, *Nature*, *374*, 34-39, 1995.

Isaak, D.G., High-temperature elasticity of iron-bearing olivines, *J. Geophys. Res.*, *97*, 871-1885, 1992.

Jackson, I., and S.M. Rigden, Composition and temperature of the Earth's mantle: Seismological models interpreted through experimental studies of Earth materials, in *The Earth's Mantle: Composition, Structure and Evolution*, edited by I. Jackson, pp. 405-460, Cambridge Univ. Press, New York, 1998.

Jackson, I., R.L. Rudnick, S.Y. O'Reilly, and C. Bezant, Measured and calculated elastic wave velocities for xenoliths from the lower crust and upper mantle, *Tectonophysics*, *173*, 207-210, 1990.

Jones, A.P., J.V. Smith, J.B. Dawson, and E.C. Hansen, Metamorphism, partial melting, and K-metasomatism of garnet-scapolite-kyanite granulite xenoliths from Lashaine, Tanzania, *J. Geol.*, *91*, 143-165, 1983.

Jordan, T.H., Mineralogies, densities and seismic velocities of garnet lherzolites and their geophysical implications, in *The Mantle Sample: Inclusions in Kimberlites and Other Volcanics*, edited by F.R. Boyd and H.O.A. Myer, pp. 1-14, AGU, Washington, D. C., 1979.

Jordan, T.H., Structure and formation of the continental tectosphere, *J. Petrol., Special Lithosphere Issue*, 11-37, 1988.

Kampfmann, W., and H. Berckhemer, High temperature experiments on the elastic and anelastic behavior of magmatic rocks, *Phys. Earth Planet. Inter.*, *40*, 223-247, 1985.

Kandelin, J., and D.J. Weidner, Elastic properties of hedenbergite, *J. Geophys. Res.*, *93*, 1063, 1988.

Karato, S., Importance of anelasticity in the interpretation of scismic tomography, *Geophys. Res. Lett.*, *20*, 1623-1626, 1993.

Karato, S., and H. Jung, Water, partial melting and the origin of the seismic low velocity and high attenuation zone in the upper mantle, *Earth Planet. Sci. Lett.*, *157*, 193-207, 1998.

Karato, S., and H.A. Spetzler, Defect microdynamics in minerals and solid-state mechanisms of seismic wave attenuation and velocity dispersion in the mantle, *Rev. Geophys.*, *28*, 399-421, 1990.

Kawamoto, T., and J.R. Holloway, Melting temperature and partial melt chemistry of H_2O-saturated mantle peridotite to 11 gigapascals, *Science*, *276*, 240-243, 1997.

Kennett, B.L.N., E.R. Engdahl, and R. Buland, Constraints on seismic velocities in the Earth from traveltimes, *Geophys. J. Int.*, *122*, 108-124, 1995.

Kennett, B.L.N., S. Widiyantoro, and R.D. van der Hilst, Joint seismic tomography for bulk sound and shear wave speed in the Earth's mantle, *J. Geophys. Res.*, *103*, 12,469-12,493, 1998.

Kirby, S.H., Rheology of the lithosphere, *Rev. Geophys.*, *21*, 1458-1487, 1983.

Leven, J.H., I. Jackson, and A.E. Ringwood, Upper mantle seismic anisotropy and lithospheric decoupling, *Nature*, *289*, 235-239, 1981.

Levien, L., D.J. Weidner, and C.T. Prewitt, Elasticity of diopside, *Phys. Chem. Miner.*, *4*, 105-113, 1979.

Marquering, H., and R. Snieder, Shear-wave velocity structure beneath Europe, the northeastern Atlantic and western Asia from waveform inversions including surface-wave mode coupling, *Geophys. J. Int.*, *124*, 283-304, 1996.

Marquering, H., R. Snieder, and G. Nolet, Waveform inversions and the significance of surface-wave mode coupling, *Geophys. J. Int.*, *124*, 258-278, 1996.

Mavko, G.M., Velocity and attenuation in partially molten rocks, *J. Geophys. Res.*, *85*, 5173-5189, 1980.

McDonough, W.F., Constraints on the composition of the continental lithospheric mantle, *Earth Planet. Sci. Lett.*, *101*, 1-18, 1990.

McKenzie, D., and M.J. Bickle, The volume and composition of melt generated by extension of the lithosphere, *J. Petrol.*, *29*, 625-679, 1988.

Meissner, R., T. Wever, and E.R. Flüh, The Moho in Europe-Implications for crustal development, *Ann. Geophys., Ser. B*, *5*, 357-364, 1987.

Meng, Y., et al., In situ high P-T X ray diffraction studies on three polymorphs (α,β,γ) of Mg_2SiO_4, *J. Geophys. Res.*, *98*, 22,199-22,207, 1993.

Minster, J.B., and D.L. Anderson, A model of dislocation-controlled rheology for the mantle, *Philos. Trans. R. Soc. London*, *299*, 319-356, 1981.

Mitchell, B.J., Anelastic structure and evolution of the continental crust and upper mantle from seismic surface wave attenuation, *Rev. Geophys.*, *33*, 441-462, 1995.

Mooney, W.D., G. Laske, and T.G. Masters, CRUST5.1: A global crustal model at 5^o x 5^o, *J. Geophys. Res.*, *103*, 727-747, 1998.

Nataf, H.C., and Y. Ricard, 3SMAC: An a priori tomographic model of the upper mantle based on geophysical modeling, *Phys. Earth Planet. Inter.*, *95*, 101-122, 1996.

Niu, Y., Mantle melting and melt extraction processes beneath ocean ridges: Evidence from abyssal peridotites, *J. Petrol.*, *38*, 1047-1074, 1997.

Nolet, G., and A. Zielhuis, Low *S* velocities under the Tornquist-Teisseyre zone: Evidence for water injection into the transition zone by subduction, *J. Geophys. Res.*, *99*, 15,813-15,820, 1994.

O'Reilly, S.Y., and W.L. Griffin, 4-D lithosphere mapping: methodology and examples, *Tectonophysics*, *262*, 3-18, 1996.

O'Reilly, S.Y., I. Jackson, and C. Bezant, Equilibrium temperatures and elastic wave velocities for upper mantle rocks from eastern Australia: Implications for the interpretation of seismological models, *Tectonophysics*, *185*, 67-82, 1990.

Panza, G.F., Lateral variations in the lithosphere in correspondence of the Southern segment of EGT, in *Second EGT Workshop: The Southern Segment*, edited by D.A. Galson and S. Mueller, pp. 47-51, Eur. Sci. Found., Strasbourg, France, 1985.

Panza, G.F., S. Mueller, and G. Calcagnile, The gross features of the lithosphere-asthenosphere system in Europe from seismic surface waves and body waves., *Pure Appl. Geophys.*, *118*, 1209-1213, 1980.

Pollack, H.N., and D.S. Chapman, On the regional variation of heat flow, geotherms and lithospheric thickness, *Tectonophysics*, *38*, 279-296, 1977.

Pollack, H.N., S.J. Hurter, and J.R. Johnson, Heat flow from the Earth's interior: Analysis of the global data set, *Rev. Geophys.*, *31*, 267-280, 1993.

Popp, T., and H. Kern, Thermal hydration reaction characterised by combined measurements of electrical conductivity and elastic wave velocities, *Earth Planet. Sci. Lett.*, *120*, 43-57, 1993.

Ranalli, G., Nonlinear flexure and equivalent mechanical thickness of the lithosphere, *Tectonophysics*, *240*, 107-114, 1994.

Ranalli, G., Seismic tomography and mineral physics, in *Seismic Modelling of Earth Structure*, edited by E. Boschi et al., pp. 443-459, Ist. Naz. di Geof., Bologna, Italy, 1996.

Ricard, Y., H.-C. Nataf, and J.-P. Montagner, The three-dimensional seismological model a priori constrained: Confrontation with seismic data, *J. Geophys. Res.*, *101*, 8457-8472, 1996.

Robertson, G.S., and J.H. Woodhouse, Comparison of *P* and *S* station corrections and their relationship to upper mantle temperatures, *J. Geophys. Res.*, *102*, 27,355-27,366, 1997.

Roosendaal, E.A., The effect of peridotite composition on elastic seismic velocities in the upper mantle, M.Sc. thesis, Utrecht Univ., Utrecht, Netherlands, 1998.

Sato, H., Thermal structure of the mantle wedge beneath northeastern Japan: Magmatism in an island arc from combined data of seismic anelasticity and velocity and heat flow, *J. Volcanol. Geotherm. Res.*, *51*, 237-252, 1992.

Sato, H., I.S. Sacks, and T. Murase, The use of laboratory velocity data for estimating temperature and partial melt fraction in the low-velocity zone: Comparison with heat flow and electrical conductivity studies, *J. Geophys. Res.*, *94*, 5689-5704, 1989.

Saxena, S.K., and G. Shen, Assessed data on heat capacity, thermal expansion, and compressibility for some oxides and silicates, *J. Geophys. Res.*, *97*, 19,813-19,825, 1992.

Schmeling, H., Numerical models on the influence of partial melt on

elastic, anelastic and electric properties of rocks, part 1, Elasticity and anelasticity, *Phys. Earth Planet. Inter.*, *41*, 34-57, 1985.

Sobolev, S.V., H. Zeyen, G. Stoll, F. Werling, R. Altherr, and K. Fuchs, Upper mantle temperatures from teleseismic tomography of French Massif Central including effects of composition, mineral reactions, anharmonicity, anelasticity and partial melt, *Earth Planet. Sci. Lett.*, *139*, 147-163, 1996.

Sobolev, S.V., H. Zeyen, M. Granet, U. Achauer, C. Bauer, F. Werling, R. Altherr, and K. Fuchs, Upper mantle temperatures and lithosphere-asthenosphere system beneath the French Massif Central constrained by seismic, gravity, petrologic and thermal observations, *Tectonophysics*, *275*, 143-164, 1997.

Spakman, W., and H. Bijwaard, Irregular cell parametrization for large tomographic problems (abstract), *Ann. Geophys.*, *16*, 28, 1998.

Spakman, W., S. van der Lee, and R.D. van der Hilst, Travel-time tomography of the European-Mediterranean mantle down to 1400 km, *Phys. Earth Planet. Inter.*, *79*, 3-74, 1993.

Sumino, Y., and O.L. Anderson, Elastic constants of minerals, in *Handbook of Physical Properties of Rocks*, edited by R.S. Carmichael, pp. 39-113, CRC Press, Boca Raton, FLa., 1984.

Thompson, A.B., Water in the Earth's upper mantle, *Nature*, *358*, 295-302, 1992.

Tralli, D.M., and J.J. Ita, Regionalized temperature variations in the upper 400 km of the Earth's mantle, *Phys. Earth Planet. Inter.*, *91*, 177-186, 1995.

Umino, N., and A. Hasegawa, Three-dimensional Q_S structure in the northeastern Japan arc, *J. Seismol. Soc. Jpn.*, *37*, 217-228, 1984.

Vacher, P., A. Mocquet, and C. Sotin, Comparison between tomographic structures and models of convection in the upper mantle, *Geophys. J. Int.*, *124*, 45-56, 1996.

Vacher, P., A. Mocquet, and C. Sotin, Computation of seismic profiles from mineral physics: the importance of non-olivine components for explaining the 660 depth discontinuity, *Phys. Earth Planet. Inter.*, *106*, 275-298, 1998.

Wang, H., and G. Simmons, Elasticity of some mantle crystal structures, 1, Pleonaste and hercynite spinel, *J. Geophys. Res.*, *77*, 4379-4392, 1972.

Waters, F.G., and A.J. Erlank, Assessment of the vertical extent and distribution of mantle metasomatism below Kimberley, South Africa, *J. Petrol., Special Lithosphere Issue*, 185-204, 1988.

Webb, S.L., and I. Jackson, The pressure dependence of the elastic moduli of single-crystal orthopyroxene (Mg_2SiO_4), *Eur. J. Mineral.*, *5*, 111-119, 1993.

Weidner, D.J., H. Wang, and J. Ito, Elasticity of orthoenstatite, *Phys. Eart Planet. Inter.*, *17*, 7-13, 1978.

Wessel, P., and W.H.F. Smith, New version of the generic mapping tools released, *Eos Trans. AGU*, *76*, 329, 1995.

Xie, J.K., and B.J. Mitchell, A back-projection method for imaging large-scale variations of *Lg* coda *Q* with application to continental Africa, *Geophys. J. Int.*, *100*, 161-181, 1990.

Yan, B., E.K. Graham, and K.P. Furlong, Lateral variations in upper mantle thermal structure inferred from three-dimensional seismic inversion models, *Geophys. Res. Lett.*, *16* , 449-453, 1989.

Yoneda, A., Pressure derivatives of elastic constants of single crystal MgO and $MgAl_2O_4$, *J. Phys. Earth*, *38*, 19-55, 1990.

Zeyen, H., F. Volker, V. Wehrle, K. Fuchs, S.V. Sobolev, and R. Altherr, Styles of continental rifting: crust-mantle detachment and mantle plumes, *Tectonophysics*, *278*, 329-352, 1997.

Zha, C., T.S. Duffy, R.T. Downs, H. Mao, and R.J. Hemley, Sound velocity and elasticity of single-crystal forsterite to 16 GPa, *J. Geophys. Res.*, *101*, 17,535-17,545, 1996.

Zhang, L., H. Ahsbahs, S.S. Hafner, and A. Kutoglu, Single-crystal compression and crystal structure of clinopyroxene up to 10 GPa, *Am. Mineral.*, *82*, 245-258, 1997.

Zielhuis, A., and G. Nolet, Shear-wave velocity variations in the upper mantle beneath central Europe, *Geophys. J. Int.*, *117*, 695-715, 1994.

S. Goes, Institut für Geophysik, ETH Hönggerberg, CH-8093 Zurich, Switzerland. (saskia@tomo.ig.erdw.ethz.ch)

R. Govers, Vening Meinesz Research School of Geodynamics, Utrecht University, P.O. Box 80.021, NL-3508 TA Utrecht, Netherlands. (govers@geo.uu.nl)

P. Vacher, Laboratoire Geophysique et Planétologie, Université de Nantes, BP 92208, F-44322 Nantes, France. (vacher@chimie.univ-nantes.fr)

(Received January 27, 1999; revised July 29, 1999;
accepted August 26, 1999.)